A Fundamental Equation of State for the Calculation of Thermodynamic Properties of *n*-Octane

R. Beckmüller,[1, a)] R. Span,[1] E. W. Lemmon,[2] and M. Thol[1]
[1)]*Thermodynamics, Ruhr University Bochum, Universitätsstraße 150, 44801 Bochum, Germany*
[2)]*Applied Chemicals and Materials Division, National Institute of Standards and Technology, 325 Broadway, Boulder, CO 80305, USA*

(Dated: September 19, 2022)

An empirical equation of state in terms of the Helmholtz energy is presented for *n*-octane. It is valid from the triple point temperature 216.37 K to 650 K with a maximum pressure of 1000 MPa and allows for the calculation of all thermodynamic properties in the vapor and liquid phase, in the supercritical region, and in equilibrium states. In the homogeneous liquid phase, the uncertainty in density is 0.03 % at atmospheric pressure. For pressures up to 200 MPa and temperatures between 270 K and 440 K, density is described with an uncertainty of 0.1 %. Outside this region, the uncertainty in the liquid phase increases to 0.5 %. Densities in the vapor phase are estimated to be accurate within 0.5 %. The uncertainty in vapor pressure depends on the temperature range and varies from 0.02 % to 0.4 %. Speed of sound in the liquid phase at temperatures below 500 K is described with an uncertainty of 0.1 % or less. The isobaric heat capacity in the liquid phase can be calculated with an uncertainty of 0.1 % and in the gas phase with 0.2 %. A reasonable physical behavior of the equation of state was ensured by the analysis of numerous thermodynamic properties.

Key words: alkane, equation of state; Helmholtz energy; *n*-octane; thermodynamic properties.

Contents

List of Figures

[a)]Electronic mail: R.Beckmueller@thermo.rub.de

List of Tables

1. Introduction

n-octane (C_8H_{18}) is the eighth *n*-alkane of the homologous series of straight-chained paraffins and internationally listed under the Chemical Abstract Service Registry Number (CASRN) 111-65-9. The aliphatic hydrocarbon is a colorless liquid at atmospheric conditions and highly flammable. The health hazards of the nonpolar lipophilic fluid range from irritations of eyes and respiratory tract to neurotoxic effects on the central nervous system. Moreover, *n*-octane is classified as very toxic to the aquatic environment. Due to these characteristics, special regulations apply for the transport and storage of *n*-octane.[1]

n-octane is mainly extracted by fractional distillation during the processing of petroleum and used as a feedstock for the production of other chemicals, e.g., solvents or cleaning agents. Furthermore, *n*-octane and its branched isomers are elementary components of fuels and lubricating oils. Even though it is usually only present as a trace element in fuels, its impact on the thermodynamic properties of the fuels is relevant and has to be considered for the most accurate description of the mixture. Especially for the design and operation of the natural gas grid, highly accurate and reliable thermophysical properties of all components are required. To provide these fluid-specific properties, a new fundamental equation of state (EOS) for *n*-octane is presented in this work.

The current reference model for *n*-octane was developed by Span and Wagner[2] in 2003. In addition to the properties of *n*-octane, the generalized EOS allows for the description of 14 other non- and weakly polar fluids. Due to its wide range of validity, high numerical stability, and outstanding performance in comparison to other technical equations, the equation of Span and Wagner[2] was established as a standard for non- and weakly-polar fluids. Consequently, the EOS of Span and Wagner[2] was used as a benchmark for the development of the new EOS for *n*-octane. However, even though the work Span and Wagner[2] is considered an outstanding contribution to the development of EOS, their model offers potential for improvement from today's perspective. Not only were more than 150 new datsets published over the last two decades, providing more accurate insights into the thermodynamic behavior of *n*-octane and covering a wider temperature and pressure range, but the modeling techniques also improved significantly in this times. The non-linear fitting algorithm used in this work was developed by Lemmon and Jacobsen[3] in 2005 and has been under continuous development since then. Thus, the knowledge gained from the development of numerous reference pure-fluid EOS[4,5] and mixture models[6] was incorporated into this work. Combined with the more comprehensive database, the main objectives of this work were to improve the description of caloric properties and to extend the range of validity while maintaining at least the same accuracy in the description of thermal properties. The obtained results are presented in the following in tabular and graphical form.

2. Equation of State and Ancillary Equations

The present EOS is formulated in terms of the Helmholtz energy a as a function of density ρ and temperature T. The formulation allows for the calculation of all thermal and caloric properties for all fluid states by combining partial derivatives of the Helmholtz energy. Detailed information about the mathematical correlations can be found, for example, in Span[7] or GERG-2004.[8] To simplify calculations, the functional form is explicit in a dimensionless form, where the Helmholtz energy is reduced by the molar gas constant R and temperature T

$$\frac{a(T,\rho)}{RT} = \alpha(\tau,\delta) \tag{1}$$

with the reciprocal reduced temperature $\tau = T_c/T$ and the reduced density $\delta = \rho/\rho_c$ as independent variables. The critical parameters T_c and ρ_c, the molar gas constant, and other characteristic thermodynamic properties of *n*-octane are listed in Table 1. The reduced Helmholtz energy α is composed of an ideal-gas contribution $\alpha^o(\tau,\delta)$ and a residual part $\alpha^r(\tau,\delta)$, where the ideal-gas part describes the properties of a hypothetical ideal gas and the residual part considers the molecular interactions of the real fluid

$$\alpha(\tau,\delta) = \alpha^o(T,\rho) + \alpha^r(\tau,\delta). \tag{2}$$

2.1. Ideal-gas contribution to the Helmholtz energy

The ideal-gas part of the Helmholtz energy is defined as

$$a^o(T,\rho) = u^o - Ts^o(T,\rho) \tag{3}$$

where the ideal-gas internal energy reads

$$u^o(T) = u_0^o + \int_{T_0}^{T} (c_p^o - R)\mathrm{d}T \tag{4}$$

and the ideal-gas entropy is

$$s^o(T,\rho) = s_0^o + \int_{T_0}^{T} \frac{(c_p^o - R)}{T}\mathrm{d}T - R\ln\left(\frac{\rho}{\rho_0}\right). \tag{5}$$

The isobaric heat capacity of the ideal gas c_p^o can be described as

$$\frac{c_p^o}{R} = n_0 + \sum_{i=1}^{3} m_i \left(\frac{\Theta_i}{T}\right)^2 \frac{\exp(\Theta_i/T)}{[\exp(\Theta_i/T)-1]^2}. \tag{6}$$

Under the simplified assumptions of a rigid rotator, the energy of a molecule stored by translation and rotation is summarized by the temperature-independent part n_0 of Eq. (6). The temperature-dependent contribution by internal vibrations and other errors due to the simplifications are modelled with so-called "Planck-Einstein terms", which are represented by the sum in Eq. (6). In this work, the empirical parameters Θ_i and m_i were fitted to ideal-gas isobaric heat capacity data

Table 1. Molar gas constant and characteristic properties of *n*-octane.

Physical property	Value	Unit	Reference
Critical temperature T_c	568.74	K	Kreglewski & Kay[9]
Critical density ρ_c	2.031	mol dm^{-3}	Kreglewski & Kay[9]
Critical pressure p_c	2.48359	MPa	This work
Normal-boiling-point temperature T_b	398.794	K	This work
Triple-point temperature T_{tp}	216.37	K	Ott & Goates[10]
Triple-point density ρ_{tp}	6.682	mol dm^{-3}	This work
Molar mass M	114.2285	g mol^{-1}	Wieser *et al.*[11]
Molar gas constant R	8.314462618	J mol^{-1} K^{-1}	CODATA[12]

from Hossenlopp and Scott[13] and Pitzer.[14] However, since the ideal-gas part and the residual part of the Helmholtz energy were simultaneously fitted and both parts contribute to the calculation of caloric properties, the parameters were also affected by fitting speed of sound and heat capacity data of the real fluid. Combining Eqs. (3) to (6) and reducing the temperature with the critical properties (see Table 1) yields the dimensionless ideal part of the Helmholtz energy, cf. Eq. (7). The corresponding parameters are listed in Table 2.

$$\alpha^{o}(\tau,\delta) = c^{II} + c^{I}\tau + (n_0 - 1)\ln(\tau) + \sum_{i=1}^{3} m_i \ln[1 - \exp(-\Theta_i \tau / T_c)] + \ln(\delta) \qquad (7)$$

The integration constants c^{I} and c^{II} define an arbitrary reference state, where the internal energy and entropy are set to zero. In this work, the saturated liquid at the normal boiling point (NBP) was chosen as the reference state.

Table 2. Parameters of the ideal-gas part α^{o} of the EOS for *n*-octane; cf. Eq. (7).

i	m_i	Θ_i / K
1	17.47	380
2	33.25	1724
3	15.63	3881
n_0	4	
c^{I}	−4.06060362648397	
c^{II}	16.93282505786505	

2.2. Residual contribution to the Helmholtz energy

The residual part of the Helmholtz energy considers intermolecular interactions. Consequently, it describes the behavior of the real fluid deviating from the hypothetical ideal gas. The complexity of this deviation does not allow a theoretically based formulation. Therefore, the residual part is empirically adjusted to experimental data from the literature. For *n*-octane, the residual part of the presented EOS consists of five polynomial-like, five exponential, and four Gaussian bell-shaped terms and reads

$$\alpha^{r}(\tau,\delta) = \sum_{i=1}^{5} n_i \delta^{d_i} \tau^{t_i} + \sum_{i=6}^{10} n_i \delta^{d_i} \tau^{t_i} \exp(-\delta^{l_i}) + \sum_{i=11}^{14} n_i \delta^{d_i} \tau^{t_i} \exp[-\eta_i(\delta - \varepsilon_i)^2 - \beta_i(\tau - \gamma_i)^2]. \qquad (8)$$

For the adjustment of the parameters n_i, d_i, t_i, l_i, η_i, ε_i, β_i, and γ_i, a non-linear fitting algorithm developed by Lemmon and Jacobsen[3] was used. The algorithm enables the simultaneous optimization of the adjustable parameters of the ideal-gas and residual part to achieve the best possible agreement between values calculated from the EOS and selected experimental data points. The impact of the selected data points is controlled by individually specified weighting factors, which are chosen by the correlator depending on the type, fluid region, and experimental uncertainty of the data point. In extremely high or low temperature and pressure regions, in which experimental data are often quite limited, physically correct behavior of the EOS is obtained by applying thermodynamic constraints. For more details, see, e.g., Lemmon *et al.*[4] and Thol *et al.*[6] The parameters of the residual part according to Eq. (8) are listed in Table 3.

2.3. Ancillary equations

Since saturation properties along the phase boundary are iteratively determined by applying the Maxwell criterion to the EOS, it is beneficial to generate starting values with ancillary equations to reduce the computational time. The ancillary equations developed in this work provide approximations for the vapor pressure p_v, saturated liquid density ρ', and saturated vapor density ρ''. As illustrated in Fig. 1, saturation properties calculated with the ancillary equations deviate within 0.02 % from the EOS over a wide temperature range. Near the critical temperature (T_c = 567.74 K), the deviations increase up to 0.04 %. Thus, the ancillary equations provide good starting values to speed up the iterative procedure of determining properties along the saturation curve. The respective parameters of Eqs. (9) to (11) are listed in Table 4.

$$\ln\left(\frac{p_v}{p_c}\right) = \left(\frac{T_c}{T}\right) \sum_{i=1}^{5} n_i \left(1 - \frac{T}{T_c}\right)^{t_i} \qquad (9)$$

Table 3. Parameters of the residual part α^{r} of the EOS for *n*-octane; cf. Eq. (8).

i	n_i	t_i	d_i	l_i	η_i	β_i	γ_i	ε_i
1	0.042240369	1	4					
2	1.4800888	0.243	1					
3	−2.0975357	0.856	1					
4	−0.72303256	1.07	2					
5	0.26084383	0.52	3					
6	−1.6713762	2.3	1	2				
7	−1.3023632	2.55	3	2				
8	0.67710461	1.075	2	1				
9	−1.1644509	2.24	2	2				
10	−0.030939987	0.951	7	1				
11	3.1437871	0.59	1		0.985	1.52	1.448	0.989
12	−0.011637891	0.917	1		13.6	998	1.08	0.986
13	−0.95649696	1.05	3		1.03	1.57	1.185	0.532
14	−0.36897912	1.634	2		1.084	1.44	1.3	1.16

$$\frac{\rho'}{\rho_{\mathrm{c}}} = 1 + \sum_{i=1}^{6} n_i \left(1 - \frac{T}{T_{\mathrm{c}}}\right)^{t_i} \tag{10}$$

$$\ln\left(\frac{\rho''}{\rho_{\mathrm{c}}}\right) = \sum_{i=1}^{6} n_i \left(1 - \frac{T}{T_{\mathrm{c}}}\right)^{t_i} \tag{11}$$

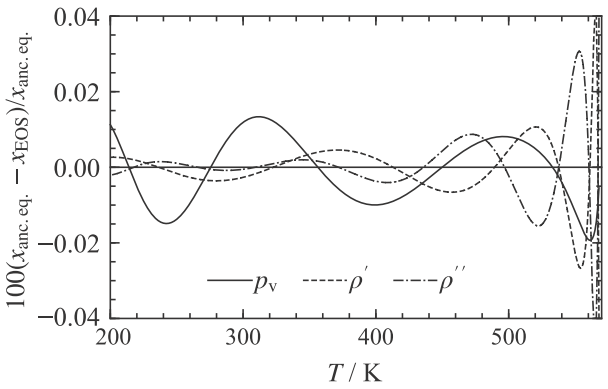

Figure 1. Percentage deviation of values calculated with the ancillary equations for vapor pressure p_{v}, saturated liquid ρ', and saturated vapor density ρ'' from the EOS.

Table 4. Parameters of the ancillary equations for the vapor pressure p_{v}, saturated liquid ρ', and saturated vapor density ρ''; cf. Eqs. (9) to (11).

	p_{v}		ρ'		ρ''	
i	n_i	t_i	n_i	t_i	n_i	t_i
1	−8.09474	1.0	2.2946	0.358	−3.18016	0.394
2	2.6247	1.5	2.6596	1.568	−7.70809	1.249
3	−2.3855	1.99	−8.4135	2.3	−24.2673	3.32
4	−4.42236	3.95	14.251	3.02	−59.814	6.715
5	−2.8186	15.5	−11.59	3.815	−138.757	14.2
6			4.0217	4.78	−487.182	31.1

3. Comparison of the Equation of State to Experimental Data

To validate the new EOS and to estimate its uncertainty in different state regions, calculated values from the EOS are compared to experimentally determined data from the literature. The representation of the available database is analyzed and discussed in this section. In total, the database consists of more than 7700 experimental state points comprising various thermodynamic properties. An overview of the database including the number of fitted data points is given in Table 5. Figure 2 shows the available homogeneous density, speed of sound, and isobaric heat capacity data in a p,T-diagram. Due to the high number of available publications, only homogeneous density and vapor-pressure datasets with more than three data points and speed of sound datasets with more than two data points are considered in this work. All considered experimental values were converted from the original publications to molar-based SI units with temperatures on the ITS-90 scale. Based on the available data, the range of validity of the new equation of state was determined to be from the triple point temperature T_{tp} = 216.37 K to T_{max} = 650 K with a maximum pressure of p_{max} = 1000 MPa.

For the statistical analysis of the database, the relative deviation ΔX of each experimental data point x_{DATA} to the property calculated from the EOS x_{EOS} was evaluated by

$$\Delta X = 100 \frac{x_{\mathrm{DATA}} - x_{\mathrm{EOS}}}{x_{\mathrm{DATA}}}. \tag{12}$$

To compare deviations of entire datasets, the average absolute relative deviation (AARD) is defined as

$$\mathrm{AARD} = \frac{1}{N} \sum_{i=1}^{N} |\Delta X_i|, \tag{13}$$

where N is the number of data points of each dataset. For datasets that comprise data points in different state regions, separate values of the AARD are provided. For this purpose, the homogeneous region is categorized into gas phase, liquid phase, critical region, and supercritical region. Furthermore, the supercritical region is separated into a low-density

Table 5. Summary of the available experimental data including number of fitted data points.

Property	Available data points	Fitted data points
Density $p\rho T$	4441	75
Vapor pressure p_v	682	17
Speed of sound w	1096	39
Isobaric heat capactiy c_p	376	15
Isobaric heat capactiy of the ideal gas c_p^o	46	3
Isochoric heat capactiy c_v	264	...
Second thermal virial coeffficient B	77	...
Third thermal virial coeffficient C	6	...
Saturated liquid density ρ'	131	3
Saturated vapor density ρ''	78	...
Enthalpy of vaporization h_vap	71	...
Isothermal compressibility κ_T	242	...
Isentropic compressibility κ_s	51	...
Isobaric thermal expansivity α_v	148	...

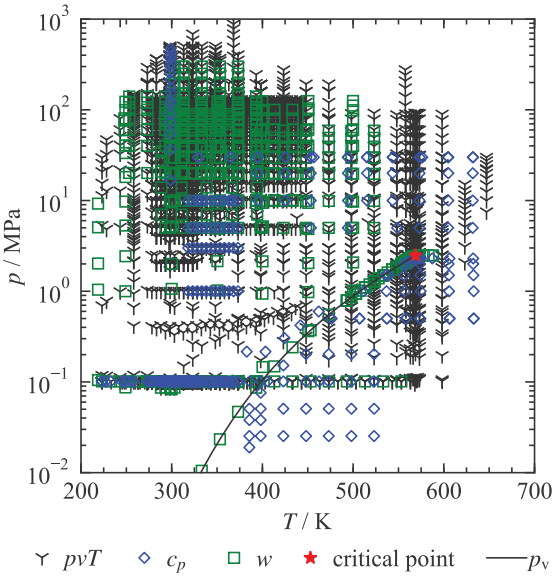

Figure 2. p,T-diagram showing the vapor pressure curve (p_v) of *n*-octane and the available homogeneous density ($p\rho T$), speed of sound (w), and isobaric heat capacity data (c_p).

(LD: $\rho/\rho_\mathrm{c} < 0.6$), medium-density (MD: $0.6 \leq \rho/\rho_\mathrm{c} \leq 1.5$), and high-density (HD: $\rho/\rho_\mathrm{c} > 1.5$) range. Thermal saturation properties are separated into a low-temperature (LT: $T/T_\mathrm{c} < 0.6$), medium-temperature (MT: $0.6 \leq T/T_\mathrm{c} \leq 0.98$), and high-temperature (HT: $T/T_\mathrm{c} > 0.98$) range.

3.1. Isobaric heat capacity of the ideal gas

The isobaric heat capacity of the ideal gas is of special interest in the development of an EOS. As explained in Sec. 2.1, the ideal-gas part of a Helmholtz-energy model is determined by a two-fold integration of the correlation for the isobaric heat capacity of the ideal gas. Since the ideal part and its derivatives are required for the calculation of caloric properties, the ideal-gas property has a crucial impact on the calculation of properties of the real fluid. For *n*-octane, the available database for the development of an equation for the ideal-gas part comprises results from statistical thermodynamics as well as data extrapolated from experimentally determined caloric properties. An overview of the datasets including their corresponding temperature ranges and deviations from the EOS is given in Table 6 and presented in Fig. 3.

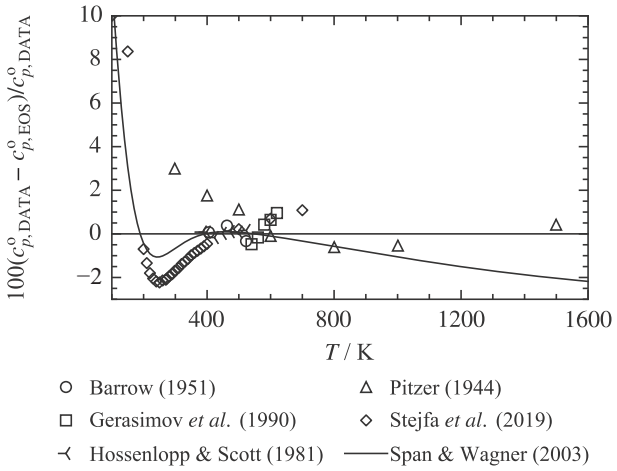

Figure 3. Percentage deviation of isobaric heat capacity data of the ideal gas from the new EOS and the EOS of Span and Wagner.[2]

In the temperature range between 380 K and 550 K, where the majority of the available data are located, the new EOS was fitted to the results of Hossenlopp and Scott,[13] who derived the heat capacity in the ideal-gas state from vapor-flow calorimetry data with an estimated uncertainty of 0.2 %. With a maximum deviation of 0.16 %, all data are described within their uncertainty. In the high-temperature range, only Pitzer[14] provides calculated data up to 1500 K. However, since the data contradict the results of Stefja *et al.*[17] in the low-temperature region, only a single data point was fitted with low weight. Stefja *et al.*[17] calculated ideal-gas properties down to 100 K with a statistical thermodynamic model called R1SM. Based on a comprehensive and detailed analysis of the sources of uncertainty, they estimated the overall uncertainty of their results for *n*-octane to be 0.7 %. However, at both the upper and lower ends of the temperature range, the data cannot be reproduced within their specified uncertainty, which is also related to a contradictory trend to the data of Hossenlopp and Scott.[13] While the EOS of Span and Wagner[2] follows the data at least qualitatively, isobaric heat capacities calculated with the new EOS deviate by up to 10 %. Thereby, it is important to state that Span and Wagner[2] developed the ideal part of their EOS independently from the residual part, whereas in this work both parts were fitted simultaneously. Consequently, the fitted caloric properties of the real fluid also affected the ideal-gas parameters of the new EOS. Since the results of Pitzer[14] and Stefja *et al.*[17] differ significantly and exhibit different trends at temperatures below 500 K, but highly accurate speed of sound and heat capacity data are available down to 250 K (see Secs. 3.8 and 3.9), we focused our work on the best possi-

Table 6. AARD of isobaric heat capacity data of the ideal gas calculated with the new EOS and the EOS of Span and Wagner.[2]

Reference	N	(T_{min} - T_{max}) / K	$AARD_{SW}$	$AARD_{This\ work}$
Barrow (1951)[15]	3	405 - 523	0.26	0.23
Gerasimov *et al*. (1990)[16]	5	539 - 620	0.53	0.59
Hossenlopp & Scott (1981)[13]	7	385 - 524	0.099	0.088
Pitzer (1944)[14]	7	298 - 1500	1.1	1.3
Stejfa *et al*. (2019)[17]	24	100 - 700	1.4	0.90

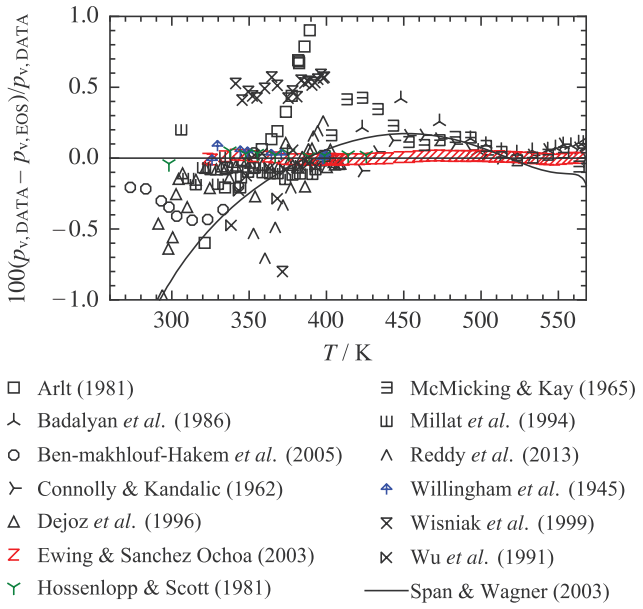

Figure 4. Percentage deviation of selected vapor-pressure data from the new EOS and the EOS of Span and Wagner.[2]

ble description of the properties of the real fluid. Nevertheless, new independent ideal-gas heat capacity data would be very valuable for validation and further improvements of the model.

3.2. Vapor pressure

With almost 700 data points from 49 publications covering the entire temprature range from the triple point up to the critical point, the vapor pressure of *n*-octane seems to be comprehensively investigated. However, depending on the sample purity and measurement technique, the experimental uncertainty of the data varies significantly. A summary of all available datasets is given in Table 7. For a better overview and analysis of the most relevant datasets, only datasets comprising 10 or more data points and a deviation of less than 1 % from the new EOS are presented in Fig. 4. A deviation diagram showing all data points can be found in the supplementary material.

Due to the outstanding consistency, the new EOS was primarily fitted to the dataset of Ewing and Sanchez Ochoa,[18] which covers a wide temperature range from 323 K up to 564 K. The vapor-pressure data were determined by comparative ebulliometry with distilled and deionized water as the reference fluid. In this process, the reference fluid and the sample under investigation were boiled in two separate cells at a common pressure while the condensation temperatures were measured. Based on the temperature measurements, the pressure of the reference fluid, which corresponds to the vapor pressure of the sample, was calculated using the reference EOS for water of Wagner and Pruß.[19] By avoiding direct pressure measurement, the accuracy of the results only depends on the thermometry and the uncertainty of the reference EOS. The uncertainty in temperature measurement is stated to be 1 mK and the uncertainty in pressure calculated from the EOS for water of Wagner and Pruß[19] is 0.015 % for pressures below 108 kPa and 0.025 % for pressure above 108 kPa. Since the contribution of the temperature uncertainty to the combined uncertainty is very small, the combined expanded uncertainty ($k = 2$) basically corresponds to the pressure uncertainty. Except for two data points in the low uncertainty region, all data points are reproduced well within their estimated uncertainty with a maximal deviation of 0.024 % and an AARD of 0.009 %.

The results of Ewing and Sanchez Ochoa[18] are confirmed in the low and medium temperature range by measurements of Hossenlopp and Scott[13] and Willingham *et al*.,[20] which are described within their experimental uncertainties with values of AARD of 0.028 % and 0.027 %, respectively. In the temperature region below 300 K, the database is highly inconsistent and no reliable data are available. The only dataset that covers temperatures down to the triple-point temperature is provided by Carruth and Kobayashi.[21] However, these data exhibit a high scatter and deviations of up to 11 %, which is why it was not used for fitting the new EOS.

The uncertainty of the new EOS in vapor pressures is estimated to be 0.03 % for temperatures above 400 K up to the critical point. Between 320 K and 400 K, the uncertainty is estimated to be 0.02 %. Due to the inconsistent data situation below 320 K, no uncertainty can be estimated for this region.

3.3. Enthalpy of vaporization

The enthalpy of vaporization was not directly considered in the fitting process of the new EOS. However, it was used to validate the vapor-pressure curve and, thus, to verify the fitted vapor-pressure data. The correlation between enthalpy of vaporization and vapor pressure is defined as follows:

$$\frac{\mathrm{d}p_\mathrm{v}}{\mathrm{d}T} = \frac{h_\mathrm{vap}}{T(v'' - v')} \tag{14}$$

Table 7. AARD of vapor-pressure data calculated with the new EOS and the EOS of Span and Wagner.[2] AARD are given for the low (LT: $T/T_c < 0.6$), medium (MT: $0.6 \leq T/T_c \leq 0.98$), and high (HT: $T/T_c > 0.98$) temperature ranges as well as the overall values.

			$AARD_{SW}$				$AARD_{This\ work}$			
Reference	N	(T_{min} - T_{max}) / K	LT	MT	HT	Overall	LT	MT	HT	Overall
Ait-Kaci *et al*. (1989)[22]	5	303 - 344	1.9	1.4	...	1.8	1.4	1.1	...	1.3
Arlt (1981)[23]	15	321 - 390	0.18	0.49	...	0.43	0.29	0.42	...	0.4
Badalyan *et al*. (1986)[24]	18	423 - 569	...	0.11	0.26	0.16	...	0.13	0.099	0.12
Batiu (1999)[25]	9	330 - 367	0.47	0.48	...	0.47	0.62	0.3	...	0.41
Ben-makhlouf-Hakem *et al*. (2005)[26]	10	273 - 354	0.51	0.18	...	0.45	0.34	0.12	...	0.3
Boukais-Belaribi *et al*. (2000)[27]	10	263 - 344	1.8	0.27	...	1.7	1.1	0.58	...	1
Carruth & Kobayashi (1973)[21]	10	216 - 298	6.7	...	...	6.7	7.8	...	...	7.8
Connolly (1965)[28]	9	463 - 544	...	0.2	...	0.2	...	0.17	...	0.17
Connolly & Kandalic (1962)[29]	15	423 - 569	...	0.073	0.16	0.084	...	0.077	0.071	0.076
Cripwell *et al*. (2016)[30]	5	380 - 381	...	0.4	...	0.4	...	0.37	...	0.37
Dejoz *et al*. (1996)[31]	39	291 - 410	0.37	0.11	...	0.22	0.27	0.062	...	0.15
Del Rio *et al*. (2002)[32]	4	298 - 329	0.84	...	...	0.84	0.27	...	...	0.27
Ewing & Sanchez Ochoa (2003)[18]	60	323 - 564	0.44	0.098	0.12	0.12	0.013	0.009	0.002	0.009
Felsing & Watson (1942)[33]	6	423 - 549	...	0.43	...	0.43	...	0.4	...	0.4
Fernandez *et al*. (2010)[34]	61	350 - 426	...	0.19	...	0.19	...	0.18	...	0.18
Gracia *et al*. (1992)[35]	9	283 - 324	1.1	...	...	1.1	0.34	...	...	0.34
Gregorowicz *et al*. (1987)[36]	15	359 - 394	...	0.057	...	0.057	...	0.076	...	0.076
Grenner *et al*. (2005)[37]	4	333 - 364	1.3	1.4	...	1.4	0.93	1.1	...	1.1
Hakem & Ait-Kaci (2002)[38]	8	263 - 354	1.2	0.62	...	1	0.82	0.88	...	0.84
Hossenlopp & Scott (1981)[13]	10	298 - 426	0.63	0.13	...	0.23	0.045	0.024	...	0.028
Jain & Yadav (1971)[39]	4	298 - 329	1.5	...	...	1.5	1.2	...	...	1.2
Jain *et al*. (1971)[39]	4	298 - 329	0.36	...	...	0.36	0.46	...	...	0.46
Koppany & Rebert (1973)[40]	7	493 - 554	...	1.5	...	1.5	...	1.5	...	1.5
Leslie & Carr (1925)[41]	6	334 - 398	8.4	6.8	...	7	8	6.7	...	6.9
Li & Li (2013)[42]	4	359 - 399	...	1.2	...	1.2	...	1.2	...	1.2
Liu & Davison (1981)[43]	4	283 - 314	2.8	...	...	2.8	3	...	...	3
McMicking & Kay (1965)[44]	18	398 - 569	...	0.093	0.17	0.1	...	0.14	0.059	0.14
Michou-Saucet *et al*. (1984)[45]	8	298 - 334	0.3	...	...	0.3	0.38	...	...	0.38
Millat *et al*. (1994)[46]	19	306 - 393	0.47	0.089	...	0.25	0.12	0.11	...	0.11
Moodley & Raal (2020)[47]	24	303 - 350	0.18	0.1	...	0.16	0.41	0.38	...	0.41
Muendel (1913)[48]	4	238 - 264	3.9	...	...	3.9	2.4	...	...	2.4
Ortega & Espiau (2003)[49]	44	368 - 416	...	0.49	...	0.49	...	0.54	...	0.54
Otsa *et al*. (1979)[50]	4	356 - 399	...	0.31	...	0.31	...	0.31	...	0.31
Perry & Thodos (1952)[51]	6	326 - 504	0.38	0.5	...	0.48	0.1	0.43	...	0.38
Plesnar *et al*. (1996)[52]	13	310 - 353	0.7	0.72	...	0.7	1	0.45	...	0.83
Reddy *et al*. (2013)[53]	11	352 - 398	...	0.2	...	0.2	...	0.27	...	0.27
Rozhnov (1967)[54]	4	303 - 414	0.6	0.37	...	0.43	0.2	0.24	...	0.23
Shevchenko & Kharchenko (1987)[55]	5	423 - 570	...	0.51	0.11	0.44	...	0.4	...	0.4
Stadnicki (1963)[56]	4	376 - 399	...	0.71	...	0.71	...	0.71	...	0.71
Wang *et al*. (2003)[57]	5	348 - 384	...	0.31	...	0.31	...	0.19	...	0.19
Willingham *et al*. (1945)[20]	10	325 - 400	0.5	0.14	...	0.21	0.051	0.021	...	0.027
Wisniak *et al*. (1999)[58]	21	341 - 399	0.85	0.58	...	0.59	...	0.52	...	0.52
Woringer (1900)[59]	26	273 - 399	17	5.7	...	12	17	5.6	...	12
Wu *et al*. (1991)[60]	12	338 - 394	0.12	0.11	...	0.11	0.47	0.096	...	0.13
Yahiaoui *et al*. (1994)[61]	4	298 - 324	1.9	...	...	1.9	1.2	...	...	1.2
Yang & Van Winkle (1955)[62]	5	323 - 399	0.17	0.3	...	0.25	0.27	0.36	...	0.32
Young (1928)[63]	14	293 - 558	1.4	0.46	...	0.8	0.76	0.46	0.5	0.57
Young (1910)[64]	30	273 - 564	0.74	0.69	0.51	0.69	1.1	0.64	0.64	0.74
Young (1900)[65]	40	269 - 398	1.1	0.53	...	0.84	1.6	0.61	...	1.2

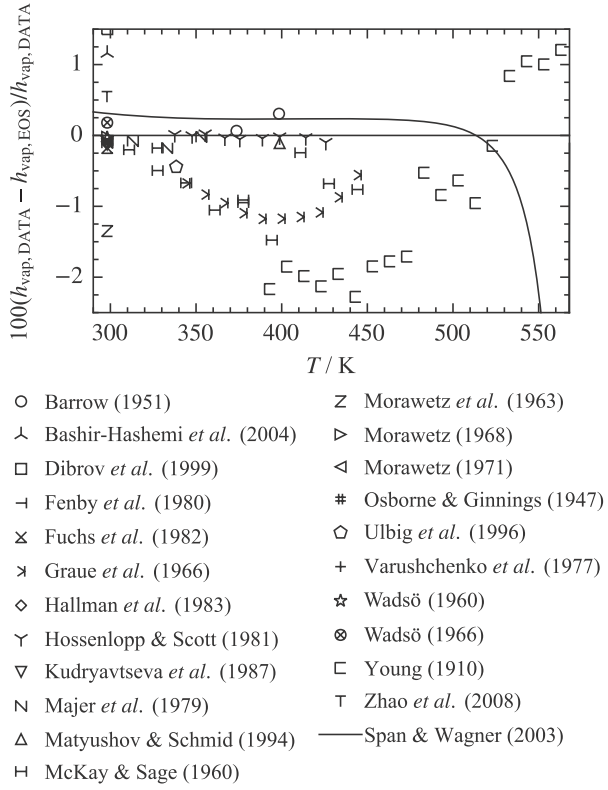

Figure 5. Percentage deviation of enthalpy of vaporization data from the new EOS and the EOS of Span and Wagner.[2]

In many studies, enthalpies of vaporization are measured along with vapor-pressure data, since the enthalpy of vaporization describes the required energy for the phase change from liquid to vapor. Figure 5 shows the percentage deviations of all available enthalpy of vaporization data.

The good reproduction of vapor-pressure data by Hossenlopp and Scott[13] is also reflected in the enthalpy of vaporization. Although none of the data points were used to fit the EOS, the data are reproduced with an AARD of 0.051 %. For their measurements, the authors used a sample with a purity of at least 99.91 mol % and the experimental uncertainty is stated to be less than 0.1 %. Their results are confirmed by the measurements of Majer *et al*.[66] The four measured data points extend over a temperature range from 298 K to 354 K with an uncertainty of 0.15 %. All data points are reproduced within their stated uncertainty with an AARD of 0.039 % and a maximum deviation of 0.14 %. Furthermore, both datasets show good agreement with measurements by Osborne and Ginnings,[67] Morawetz *et al*.,[68] and Wadsö[69] at 298 K. In the temperature range above 450 K, only data of Young[64] are available, which were measured in 1910. Information on the experimental uncertainty and sample purity is not provided. However, the data differ by up to 2 % from those of Hossenlopp and Scott[13] in the overlapping temperature range. Therefore, deviations of approximately 1 % in the high-temperature range are reasonable.

Based on the data reproduction of Hossenlopp and Scott[13] and Young,[64] the uncertainty of the new EOS for the enthalpy of vaporization is determined to be 0.1 % up to 425 K and 2 % above 425 K.

3.4. Homogeneous density

Since homogeneous density data are of great interest in a multitude of technical processes, many different approaches and apparatuses were developed in the last decades to determine this property as accurately as possible. Consequently, many datasets are available in the literature and homogeneous density data often represent the majority of the available database for the development of an EOS. Apparatuses like the two-sinker densimeter are one of the most accurate methods for determining thermodynamic properties experimentally and allow for density measurements with remarkably small uncertainties. However, validating an EOS with these data implies a reasonable and comprehensible estimation of experimental uncertainties, including temperature and pressure measurements, sample preparation and handling, apparatus preparation and calibration, etc. But experience shows that many publications lack this important information or uncertainties are estimated too optimistically. Especially when measurements are performed with commercial apparatuses, like vibrating-tube densimeters, often only the uncertainties stated by the manufacturer are reported in the publications. However, the specifications provided by the manufacturer refer to measurements under ideal conditions, i.e., atmospheric pressure and temperatures close to ambient conditions. Recent studies by Prokopova *et al*.[85] showed that just by increasing the temperature at atmospheric pressure, the uncertainty of the obtained data can be significantly higher than the accuracy stated by the manufacturer. Consequently, similar effects are also expected for pressures higher than atmospheric pressure. In addition to the increase in uncertainty caused by pressure and temperature levels above ambient conditions, sample purity and calibration of the apparatus have a significant impact on the accuracy of measurements. Fortin *et al*.[86] investigated the impact of contaminated samples on the accuracy of a vibrating-tube densimeter and pointed out the importance of a careful cleaning process of the apparatus to avoid contamination and, thus, ensure a good repeatability and reproducibility of experimental measurements. Furthermore, the authors emphasize the importance of choosing a suitable reference fluid for calibration. To minimize the experimental uncertainty, they recommend to calibrate commercial instruments regularly with several reference fluids whose properties are similar to those of the sample of interest. But even if the sample and apparatus are carefully prepared and calibrated, numerous challenges need to be overcome when performing measurements, ranging from non-uniform mass distributions of the sample along the tube to aging and thermal effects of the tube material. For more details about these challenges, see Gonzalez-Salgado *et al*.[87]

In summary, a large variety of effects can lead to non-ideal conditions of conducting measurements. Consequently, only indicating of the manufacturer uncertainties is not sufficient for an uncertainty analysis. Nevertheless, if no other information is provided in the publication, the stated uncertainties are

Table 8. AARD of enthalpy of vaporization data calculated with the new EOS and the EOS of Span and Wagner.[2] AARD are given for the low (LT: $T/T_c < 0.6$), medium (MT: $0.6 \leq T/T_c \leq 0.98$), and high (HT: $T/T_c > 0.98$) temperature ranges as well as the overall values.

			$AARD_{SW}$				$AARD_{This\ work}$			
Reference	N	(T_{min} - T_{max}) / K	LT	MT	HT	Overall	LT	MT	HT	Overall
Barrow (1951)[15]	2	373 - 399	...	0.12	...	0.12	...	0.19	...	0.19
Bashir-Hashemi *et al*. (2004)[70]	1	298.15	0.85	...	...	0.85	1.2	...	...	1.2
Dibrov *et al*. (1999)[71]	1	298.15	7.9	...	...	7.9	8.2	...	...	8.2
Fenby *et al*. (1980)[72]	1	298.19	0.38	...	...	0.38	0.072	...	...	0.072
Fuchs *et al*. (1982)[73]	1	298.14	0.49	...	...	0.49	0.18	...	...	0.18
Graue *et al*. (1966)[74]	10	344 - 445	...	1.2	...	1.2	...	0.96	...	0.96
Hallman *et al*. (1983)[75]	1	298.14	0.43	...	...	0.43	0.12	...	...	0.12
Hossenlopp & Scott (1981)[13]	10	298 - 426	0.31	0.27	...	0.28	0.04	0.039	...	0.039
Kudryavtseva *et al*. (1987)[76]	1	298.14	0.44	...	...	0.44	0.13	...	...	0.13
Majer *et al*. (1979)[66]	4	298 - 354	0.4	0.26	...	0.37	0.12	0.022	...	0.096
Matyushov & Schmid (1994)[77]	1	398.8	...	0.34	...	0.34	...	0.11	...	0.11
McKay & Sage (1960)[78]	11	310 - 445	0.56	1.1	...	0.94	0.29	0.84	...	0.69
Morawetz (1971)[79]	1	298.14	0.4	...	...	0.4	0.09	...	...	0.09
Morawetz *et al*. (1963)[80]	1	298.14	1.7	...	...	1.7	1.3	...	...	1.3
Morawetz (1968)[68]	1	298.14	0.33	...	...	0.33	0.021	...	...	0.021
Osborne & Ginnings (1947)[67]	1	298.14	0.39	...	...	0.39	0.074	...	...	0.074
Ulbig *et al*. (1996)[81]	1	338.41	0.69	...	...	0.69	0.44	...	...	0.44
Varushchenko *et al*. (1977)[82]	1	298.14	0.43	...	...	0.43	0.12	...	...	0.12
Wadsö (1960)[69]	1	298.14	0.34	...	...	0.34	0.031	...	...	0.031
Wadsö (1966)[83]	1	298.14	0.13	...	...	0.13	0.18	...	...	0.18
Young (1910)[64]	18	393 - 564	...	1.8	8.4	2.2	...	1.4	1.2	1.4
Zhao *et al*. (2008)[84]	1	298	0.23	...	...	0.23	0.54	...	...	0.54

used to calculate an overall expanded uncertainty ($k = 2$) by applying Gaussian error propagation. Moreover, it is important to keep in mind that the impact of the sample purity is not considered in the overall uncertainty, if no information about the impurities is given.

Overall, the experimental homogeneous density database comprises 4456 data points covering a temperature range from 223 K up to 647 K with pressures up to 980 MPa. The calculated AARD of each dataset are listed in Table 10, including their corresponding temperature and pressure range. Deviation diagrams of all available data divided into isotherms can be found in the supplementary material. Except for the datasets of Badalyan *et al*.[88] and Abdulagatov *et al*.,[89,90] all data are located in the liquid phase. Furthermore, 82 of the 129 available publications only contain data at atmospheric pressure. Due to the large amount of experimental data, only the most important primary datasets for the validation of the EOS are discussed in the following.

Figure 6 shows the percentage deviation from the new EOS to all datasets at atmospheric pressure with more than 10 data points. The most consistent data are provided by Cerdeiriña *et al*.[91] and Landaverde-Cortes *et al*.[92] Both research groups used vibrating-tube densimeters, which were solely calibrated for density measurements at atmospheric pressure. As mentioned at the beginning of this section, the effort for calibration and possible inaccuracies due to erroneous pressure measurement can be reduced by limiting the pressure range to ambient pressure, if the calibration is performed correctly.

For atmospheric measurements in a temperature range between 273 K and 363 K, Landaverde-Cortes *et al*.[92] used an Anton Paar DMA 5000[a] vibrating-tube densimeter, which was calibrated with water. According to the certificate of analysis, the purity of the *n*-octane sample was 99.44 mol %. Uncertainties in density and temperature are given as 3×10^{-5} g cm^{-3} and 0.01 K, respectively. Applying Gaussian error propagation, we determined a combined uncertainty of 0.0091 % ($k = 2$). However, since the composition of the sample impurities is not known, their contribution to the combined uncertainty could not be considered. The AARD of the dataset is 0.004 % with a maximum deviation of 0.012 %. Even though two data points exceed the estimated experimental uncertainty by 0.003 %, we assume a correct description of the data since the effect of sample purity is not considered in the combined uncertainty.

Cerdeiriña *et al*.[91] used an Anton Paar DAS-48 instrument to simultaneously determine density and speed of sound data. Densities were measured with a vibrating-tube densimeter and a pulse-echo-analysis was used for speed of sound measurements. Uncertainties in density and temperature were adopted from the data sheet of the manufacturer and are specified as 1×10^{-4} g cm^{-3} and 0.01 K. The sample purity was determined by a gas chromatography as > 99.5 mol %. Based on

[a] Commercial equipment, instruments, or materials are identified only in order to adequately specify certain procedures. In no case does such identification imply recommendation or endorsement by the National Institute of Standards and Technology, nor does it imply that the products identified are necessarily the best available for the purpose.

this information, a combined uncertainty of 0.029 % ($k = 2$) was calculated. The new EOS reproduces the data with an AARD of 0.004 % and a maximum deviation of 0.011 %.

The results of Landaverde-Cortes *et al.*[92] and Cerdeiriña *et al.*[91] are consistent with data of Reyes-Garcia and Iglesias-Silva.[93] However, this fact has only limited significance, since the data of Landaverde-Cortes *et al.*[92] and Reyes-Garcia and Iglesias-Silva[93] were determined with the same experimental setup and the authors worked in the same research group.

One of the most comprehensive datasets in terms of temperature was provided by Chappelow *et al.*[94] The authors measured 31 data points in the liquid phase in a temperature range from 245 K to 396 K at atmospheric pressure with a single-sinker hydrostatic weighing apparatus. To determine the density of the investigated fluid, the vacuum-corrected weight of the sinker in air and the weight of the sinker while suspended in the liquid was measured with a single-pan balance. Based on the difference between these two measurements, the liquid density was calculated with an estimated uncertainty of 1×10^{-6} g cm^{-3}. The temperature measurements were carried out with a platinum resistance thermometer with an uncertainty of 0.01 K. The purity of the *n*-octane sample is reported with 99.92 mol %. The specified uncertainties lead to a combined expanded uncertainty ($k = 2$) of 0.0025 %, which seems quite optimistic. Overall, the data are reproduced with an AARD of 0.026 % with a maximum deviation of 0.09 % by the new EOS. At temperatures above 370 K, the deviation increases significantly with a maximum at 390 K (cf. Fig. 6). This peak was present during the entire fitting process and could not be eliminated. However, since neither the dataset of Badalyan *et al.*[88] nor Abdussalam *et al.*[95] show a similar behavior in this temperature range and the entire dataset exhibits an offset to those already discussed, the peak could be an indicator of experimental error.

In the liquid phase at pressures above ambient pressure, the new EOS agrees very well with the data of Sanmamed *et al.*[96] The dataset comprises 117 data points and ranges from 283 K to 324 K at pressures up to 60 MPa. To calibrate the Anton Paar DMA512P vibrating-tube densimeter, the authors followed an approach of the Forced Path Mechanical Calibration Model, which includes rigorous physical considerations on the stress and thermal behavior of the vibrating-tube. The calibration constants of the model were determined with dodecane and tetrachloroethylene as calibration fluids at atmospheric pressure and densities of water calculated from the EOS of Wagner and Pruß[19] at higher pressures. Temperature and pressure were measured with an uncertainty of 0.005 K and 0.003 MPa, respectively. The sample was purchased with a purity of >99 mol % and degassed before use. Based on a detailed analysis, the authors specify an expanded uncertainty ($k = 2$) of 0.12 kg m^{-3} for densities at atmospheric pressure and 0.20 kg m^{-3} for higher pressures, which corresponds to relative uncertainties of 0.017 % and 0.028 %. Except for three data points at pressures >50 MPa, all data points (97.3 %) are described within their specified combined uncertainties. The AARD of the entire dataset is 0.012 % with a maximum deviation of 0.032 %.

At elevated pressures and higher temperatures, only a few

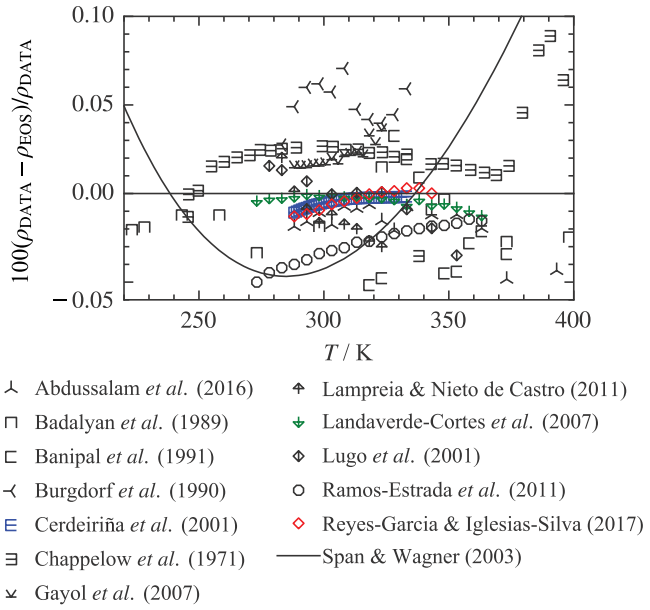

Figure 6. Percentage deviation of selected homogeneous density data at atmospheric pressure from the new EOS and the EOS of Span and Wagner.[2]

highly accurate datasets are available. One of these datasets is the set of Caudwell *et al.*[97] In the overlapping temperature and pressure region, the data are in good agreement with the data of Sanmamed *et al.*[96] Therefore, the data are considered to be a reliable extension for temperatures up to 474 K and pressures up to 202 MPa. Caudwell *et al.*[97] used a vibrating-wire instrument to measure the viscosity and density simultaneously. Parameters of the working equation of the instrument were determined by calibration measurements in ambient air and methylbenzene or derived from material properties in the literature. The expanded uncertainty of temperature and pressure measurements are stated to be 0.02 K and 0.02 MPa, while the overall relative expanded uncertainty ($k = 2$) in density is estimated to be 0.2 %. All data points are represented by the new EOS within 0.11 % with an AARD of 0.042 %.

Other comprehensive and accurate datasets are, for example, the measurements of Schedemann[98] and Lugo *et al.*[99] Both the data of Sanmamed *et al.*[96] and Caudwell *et al.*[97] agree with these datasets in overlapping temperature and pressure regions. However, while the data of Schedemann[98] confirm the data of Caudwell *et al.*[97] at temperatures above 330 K, the data of Schedemann[98] show a systematic offset from the data of Caudwell *et al.*[97] and other authors at lower temperatures (cf. Fig. 7). The data of Lugo *et al.*[99] on the other hand, agree with the data of Sanmamed *et al.*[96] at temperatures up to 330 K and deviate more with increasing temperature. Even though both authors used the identical measurement method, the data of Lugo *et al.*[99] and Schedemann[98] exhibit a systemetic offset over the entire temperature range, which increases with increasing pressure.

Lugo *et al.*[99] used an Anton Paar DMA 60/512P vibrating-tube densimeter to perform density measurements in a temperature range of 263 K to 424 K and at pressures up to 70 MPa

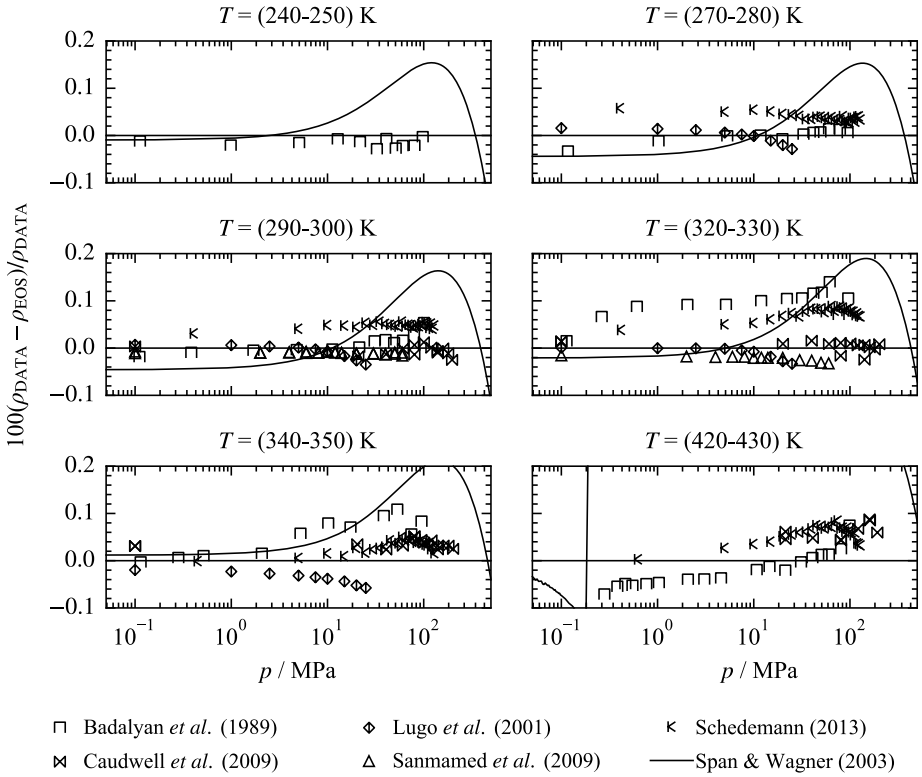

Figure 7. Percentage deviation of homogeneous density data at selected isotherms in the liquid phase from the new EOS and the EOS of Span and Wagner.[2]

with an uncertainty of 3×10^{-5} g cm^{-3}. Temperatures were measured with a platinum-resistance thermometer, which had a maximum uncertainty of 0.01 K after calibration. Pressures were determined by a manometer with an uncertainty of 0.002 MPa. The sample with a purity of at least 99.5 % was dried with molecular sieves and degassed with an ultrasonic bath before use. However, the publication does not contain information on the sample purity after these additional preparations. Considering the given measurement uncertainties, the combined uncertainty was calculated with Gaussian error propagation as 0.009 % ($k = 2$). The AARD of the entire dataset is 0.020 % with a maximum deviation of 0.065 %.

The experimental setup of Schedemann[98] consists of an Anton Paar DMA HPM vibrating-tube densimeter, which allows for measurements in a temperature range from 263 K to 473 K and pressures up to 140 MPa. According to the information of the manufacturer, the accuracy of density measurements within this state region is at least 1×10^{-4} g cm^{-3}. For temperature measurements, an external Pt100-thermometer with an uncertainty of 0.1 K was installed. In addition to the internal pressure sensor, a redundant sensor was installed, which was calibrated with a deadweight tester in a pressure range from 0.1 MPa up to 40 MPa. For pressures up to 140 MPa, the calibration was extrapolated. The sample was dried with a molecular sieve before the purity was determined with a gas chromatograph to be 99.86 %. Based on the given information, a combined uncertainty of 0.053 % ($k = 2$) was calculated. The AARD of the dataset is 0.052 % with a maximum deviation of 0.095 %.

One possible reason for the systematic offset of the datasets of Lugo *et al.*[99] and Schedemann[98] could be the chosen calibration procedures. To determine the density ρ from the experimentally recorded resonance period τ, a calibration function is required. The same basic form of this calibration function was used by both research groups and reads:

$$\rho(p,T) = A(p,T)\tau^2 - B(p,T). \tag{15}$$

However, to determine the apparatus parameters A and B, the authors used different calibration approaches. Schedemann[98] used a calibration method in which the period times of two reference fluids are measured over a wide temperature and pressure range and the associated densities are calculated with an EOS. Water and *n*-heptane were used as reference fluids. The required densities of water were determined with the EOS of Wagner and Pruß.[19] The densities of *n*-heptane in a pressure range between 30 MPa and 100 MPa were calculated with the EOS of Span and Wagner[2] and below 30 MPa with the EOS of Schilling *et al.*[100] Afterwards, the calibration parameters were adjusted to the determined data points using multilinear regression. Lugo *et al.*[99] used a calibration method developed by Lagourette *et al.*[101] The method is based on the assumption that $A(p,T)$ is only a function of temperature, i.e., $A(T)$ and only the parameter $B(p,T)$ is temperature- and pressure-dependent. The resulting calibration function was adjusted to density data of water published by Kell and Whalley.[102] This approach has the advantage that the inaccuracies, which result

from the global correlation, are avoided. However, the disadvantage is that only density data at the calibrated points can be used. Therefore, temperature and pressure must be precisely controlled at each measuring point. Besides these different calibration procedures, the systematic offset may also result from various other sources like sample handling and filling. Consequently, the cause can not be reliably identified with the given information.

In the low-temperature region ($T < 278$ K), only Badalyan *et al*.[88] provide data at elevated pressures. Overall, the authors measured 788 data points in the gas, liquid, and supercritical phase with a spherical piezometer with constant volume. The authors state uncertainties of 0.03 K and 0.05 % for temperature and pressure measurements. Density uncertainty is specified as 0.082 % for $\rho \geq 0.7\rho_c$ and 0.23 % for $\rho < 0.7\rho_c$. Detailed information, for example on the measuring equipment, could not be obtained from the Russian publication. The sample purity is given as 99.95 %. Compared to other publications from the same decade, the purity seems questionable, since such high purity can only be reached with extremely high technical and financial effort. Nevertheless, the combined uncertainties ($k = 2$) are determined to be 0.50 % at $\rho < 0.7\rho_c$ and 0.21 % at $\rho \geq 0.7\rho_c$ based on the given information. The new EOS describes the data in the gas phase with an AARD of 0.29 % and in the liquid phase with an AARD of 0.072 %. The AARD in the critical region is 1.7 %. In the supercritical region for small, medium, and high densities, the data are reproduced with an AARD of 0.22 %, 1.7 %, and 0.15 %, resulting in an overall AARD of 0.26 %.

To validate the EOS in the critical region, it is reasonable to evaluate pressure deviations instead of density deviations, since a minimal isothermal pressure change results in a large change in density. Figure 8 shows the percentage deviation in terms of pressure of the new EOS and the EOS of Span and Wagner[2] in the extended critical region (516 K to 624 K).

In the extended critical region, a total of five datasets were available, two of which were provided by the same research group.[89,103] However, the critical region is not analyzed separately in any of these publications. All authors report uncertainties that are valid for the entire homogeneous region, but experience shows that measurements in the critical region are more challenging and, therefore, uncertainties are often significantly higher. Moreover, Abdulagatov *et al*.[89] and Felsing and Watson[33] do not provide information on their sample purity. A summary of the calculated combined uncertainties and the respective AARD in terms of pressure in the extended critical region are listed in Table 9.

The significant difference between the calculated combined uncertainties and AARD in pressure of some datasets results from a systematic offset between the data. Figure 9 shows data measured by Liu *et al*.[104] at 557.55 K in comparison to data of Badalyan *et al*.[88] at 558.11 K in a pressure-density-diagram. Especially in the low-pressure range, an offset of up to 10 MPa is present, which decreases with increasing pressure. Since the new EOS was fitted to the dataset of Badalyan *et al*.[88] in the extended critical region, this offset leads to high deviations of other datasets.

To compare the new EOS and the EOS of Span and

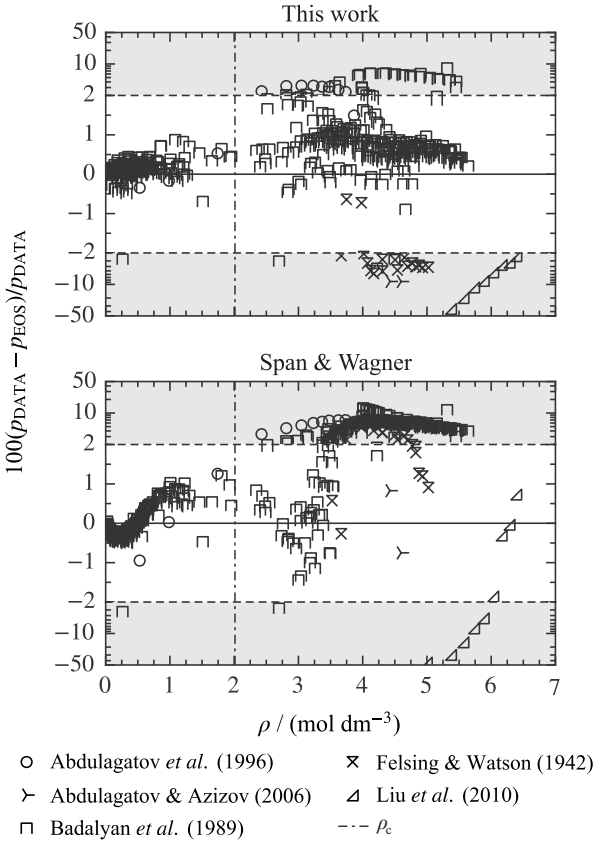

Figure 8. Percentage deviation in terms of pressure of homogeneous density data in the extended critical region from the new EOS and the EOS of Span and Wagner.[2] The ordinate is linearly scaled between the dashed lines and logarithmically scaled in the gray filled regions.

Table 9. Deviations in terms of pressure of homogeneous density data in the extended critical region.

Reference	N	Combined pressure uncertainty ($k = 2$)	AARD in pressure
Abdulagatov *et al*.[89]	2	1.76	8.61
Abdulagatov & Azizov[103]	12	0.73	2.17
Badalyan *et al*.[88]	558	0.78	0.68
Felsing & Watson[33]	19	2.33	3.29
Liu *et al*.[104]	10	11.2	20.91

Wagner[2] in regions where no experimental data are available, the percentage deviation in density between both models is illustrated over a wide temperature and pressure range in Fig. 10. The highest deviation between both models is located near the critical point and in the supercritical region at temperatures above 550 K. However, parts of this high-deviation region lie outside the range of validity of the EOS of Span and Wagner,[2] which is represented by the white dashed line. Within the high-deviation region, areas of low deviations are present, which result from a change in deviation from negative to positive or vice versa. This behavior is also present at lower temperatures, but less distinct, as illustrated in Fig. 7. High deviations in the vicinity of the critical point are attributable to

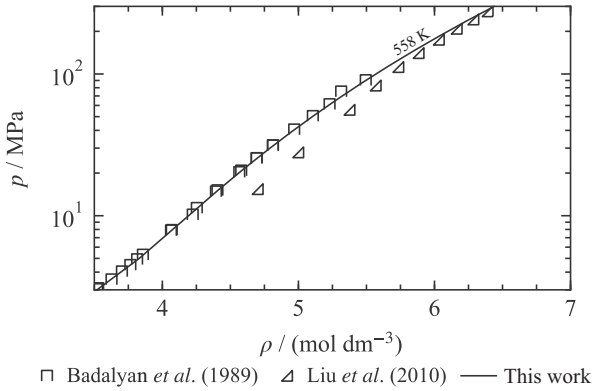

Figure 9. p,T-diagram showing selected experimental homogeneous density data in the extended critical region.

different critical properties being used for the development of the models. The model by Span and Wagner[2] is based on the critical temperature ($T_c = 569.32$ K) determined by Gomez-Nieto[105] and the critical density ($\rho_c = 2.056404$ mol dm^{-3}) of McMicking and Kay,[44] whereas the new model is based on the critical properties measured by Kreglewski and Kay[9] (see Table 1). Since only Abdulagatov *et al*.[89] and Badalyan *et al*. provide density data at supercritical temperatures and both datasets are of relatively high uncertainties, new highly accurate data are needed to validate the models in this region.

Based on the reproduction of the available density datasets and their experimental uncertainties, the uncertainty in density of the new model was estimated as a function of temperature and pressure as shown in Fig. 11. Since the entire range of validity is not covered by experimental data, uncertainty estimations are not possible for all state regions. Regions where no uncertainties could be estimated are marked in gray. At the lower temperature end, the range of validity is bordered by the solid phase. Since no model for the melting line of *n*-octane is available in the literature, the melting line was extrapolated graphically from melting temperatures published by Würflinger[106] using the following second-degree polynomial:

$$p_{\mathrm{melt}}(T) = 0.0205T^2 - 4.2957T - 27.065 \qquad (16)$$

This correlation is not related to the EOS developed in this work, but is solely used to roughly estimate the freezing curve for visualization purposes. The triangular-shaped critical region is bordered by the isochores 0.91 mol dm^{-3} and 3.3 mol dm^{-3} and the 3 MPa isobar. For this region, the uncertainty is given in terms of pressure.

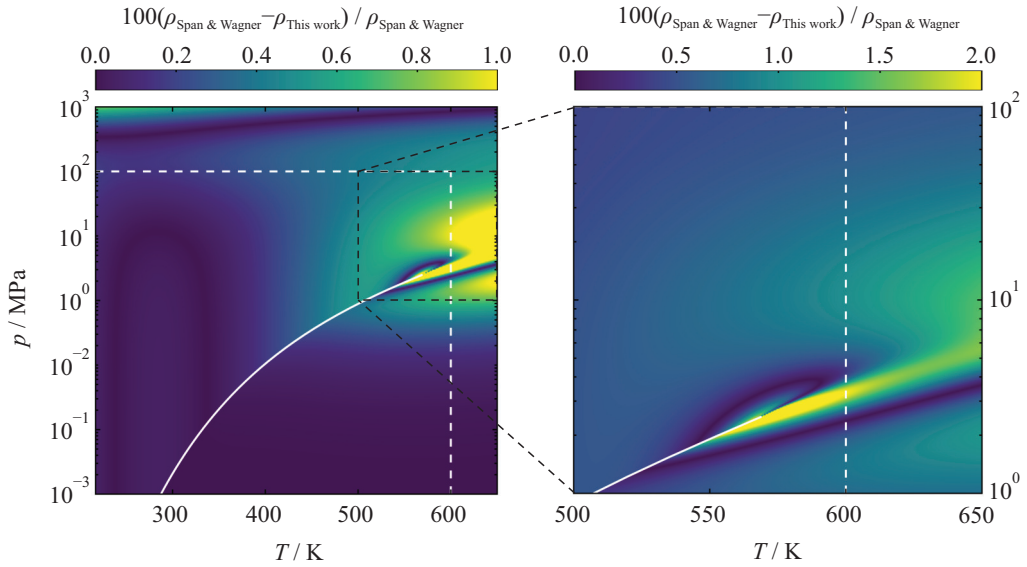

Figure 10. Percentage deviation in density in the homogeneous region between the new EOS and the EOS of Span and Wagner.[2] The white dashed lines mark the normal range of validity of the model by Span and Wagner,[2] whereas the range of the new model corresponds to the axis limits of the left diagram. The solid white curve represents the vapor-pressure curve of the new model.

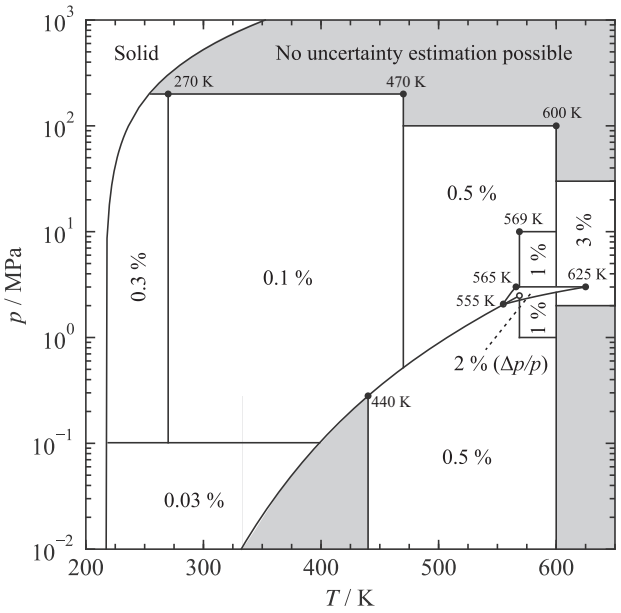

Figure 11. Estimated expanded relative uncertainties ($k = 2$) in density $\Delta\rho/\rho$ of the new EOS. Uncertainty in the critical region is given in pressure $\Delta p/p$. The critical region is bordered by the isochores 0.91 mol dm^{-3} and 3.3 mol dm^{-3} as well as the 3 MPa isobar.

Table 10: AARD of homogeneous density data calculated with the new EOS and the EOS of Span and Wagner.[2]

Reference	N	(T_{min} - T_{max}) / K	(p_{min} - p_{max}) / MPa	$AARD_{SW}$	$AARD_{This\ work}$
Abdulagatov *et al*. (1996)[89]	12	623.15	2.1 - 15.1	2.1	1.1[a]
Abdulagatov *et al*. (1998)[90]	11	647.05	7.5 - 30.0	1.6	0.50[b]
Abdulagatov & Azizov (2006)[103]	13	301 - 517	0.1 - 11.5	0.022	0.16
Abdussalam *et al*. (2016)[95]	223	288 - 414	0.1 - 60.0	0.21	0.11
Aicart *et al*. (1980)[108]	4	298 - 334	0.101325	0.046	0.021
Alonso *et al*. (2012)[109]	5	288 - 309	0.101325	0.068	0.025
Aminabhavi & Gopalakrishna (1995)[110]	4	298 - 314	0.101325	0.034	0.009
Aminabhavi *et al*. (1992)[111]	6	298 - 324	0.101325	0.27	0.25
Aminabhavi *et al*. (1994)[112]	5	298 - 319	0.101325	0.009	0.031
Asfour *et al*. (1990)[113]	4	293 - 314	0.101325	0.017	0.037
Badalyan *et al*. (1989)[88]	788	223 - 599	<0.1 - 102	0.66	0.26[c]
Banipal *et al*. (1991)[114]	66	318 - 374	0.1 - 10.0	0.075	0.044
Belonenko *et al*. (2000)[115]	23	298 - 299	0.1 - 300	0.11	0.073
Ben'kovskii *et al*. (1970)[116]	4	258 - 299	0.101325	0.051	0.022
Benson & Winnick (1971)[117]	71	258.15	0.1 - 149	0.14	0.07
Boelhouwer (1960)[118]	51	303 - 394	<0.1 - 118	0.25	0.1
Brazier & Freeman (1969)[119]	9	303.14	0.1 - 400	0.42	0.33
Bridgman (1949)[120]	11	298.14	0.1 - 491	2.2	2.2
Bridgman (1931)[121]	25	273 - 369	0.1 - 981	0.2	0.18
Burgdorf (1995)[122]	11	283 - 334	0.101325	0.083	0.051
Calvo *et al*. (1998)[123]	3	288 - 309	0.101325	0.024	0.018
Caudwell *et al*. (2009)[97]	88	298 - 474	0.1 - 202	0.19	0.042
Cerdeiriña *et al*. (2001)[91]	46	288 - 334	0.101325	0.027	0.004
Chappelow *et al*. (1971)[94]	31	245 - 396	0.101325	0.047	0.026
Chen *et al*. (2013)[124]	6	298 - 324	0.101325	0.052	0.019
Cisneros-Perez *et al*. (2012)[125]	5	293 - 314	0.101325	0.032	0.008
Cominges *et al*. (2002)[126]	5	288 - 309	0.101325	0.028	0.014
D'Aprano *et al*. (1990)[127]	5	273 - 319	0.101325	0.024	0.054
Devi *et al*. (2018)[128]	9	288 - 329	0.101325	0.054	0.02
Diaz Peña & Tardajos (1978)[129]	4	298 - 334	0.101325	0.039	0.011
Dix *et al*. (1991)[130]	22	298 - 324	0.1 - 103	0.091	0.14
Doolittle & Peterson (1951)[131]	4	263 - 374	0.101325	0.049	0.006
Dornte & Smyth (1930)[132]	9	223 - 384	0.101325	0.097	0.066
Dumitrescu *et al*. (2015)[133]	4	293 - 309	0.101325	0.11	0.093
Dymond *et al*. (1982)[134]	28	298 - 349	0.1 - 480	0.21	0.11
Dymond *et al*. (1981)[135]	41	298 - 374	0.1 - 506	0.33	0.23
Eduljee *et al*. (1951)[136]	39	273 - 334	0.1 - 507	0.47	0.39
Estrada-Baltazar *et al*. (2013)[137]	7	293 - 324	0.101325	0.025	0.01
Exarchos *et al*. (1995)[138]	5	293 - 314	0.101325	0.042	0.006
Fang *et al*. (2014)[139]	4	283 - 304	0.101325	0.041	0.003
Felsing & Watson (1942)[33]	89	373 - 549	0.5 - 30.4	0.29	0.5
Fernandez *et al*. (2010)[34]	4	291 - 329	0.101325	0.035	0.015
Fernandez *et al*. (2013)[140]	4	291 - 329	0.101325	0.035	0.014
Freyer *et al*. (1929)[141]	6	273 - 324	0.101325	2.4	2.4
Fukuchi *et al*. (1983)[142]	7	293 - 344	0.101325	0.044	0.051
Garbajosa *et al*. (1982)[143]	4	298 - 334	0.101325	0.028	0.002
Garcia-Morales *et al*. (2017)[144]	66	293 - 393	0.2 - 69.9	0.081	0.049
Garcia *et al*. (1986)[145]	5	288 - 309	0.101325	0.036	0.007
Garcia *et al*. (2002)[146]	5	278 - 319	0.101325	0.077	0.072
Gayol *et al*. (2013)[147]	18	288 - 309	0.1 - 40.0	0.068	0.029
Gayol *et al*. (2007)[107]	15	288 - 324	0.101325	0.059	0.023
Golik & Adamenko (1965)[148]	8	293 - 364	0.101325	0.11	0.14
Golik *et al*. (1972)[149]	36	303 - 394	<0.1 - 246	0.25	0.26
Gong *et al*. (2012)[150]	4	293 - 314	0.101325	0.063	0.023
Gonzalez *et al*. (1999)[151]	4	283 - 299	0.101325	0.047	0.003
Goodwin *et al*. (2006)[152]	37	348 - 424	0.1 - 68.4	0.18	0.3

Table 10: Continues on next page

Table 10 continued.

Reference	N	(T_{min} - T_{max}) / K	(p_{min} - p_{max}) / MPa	$AARD_{SW}$	$AARD_{This\ work}$
Goodwin *et al*. (1996)[153]	14	298 - 304	0.7 - 32.6	0.57	0.56
Gouel (1978)[154]	72	293 - 394	0.1 - 40.5	0.19	0.14
Gracia *et al*. (1992)[35]	9	283 - 324	0.101325	0.76	0.8
Harris *et al*. (1997)[155]	61	283 - 354	0.1 - 374	0.24	0.14
Hayduk & Wong (1990)[156]	4	278 - 324	0.1	0.055	0.056
Hussain & Moodley (2020)[157]	105	313 - 354	<0.1	1.6	1.6
Islam *et al*. (1973)[158]	7	300 - 363	0.101325	2.6	2.6
Islam & Waris (1976)[159]	7	312 - 374	0.101325	0.33	0.36
Jain & Yadav (1971)[39]	4	298 - 329	0.101325	0.019	0.049
Jimenez *et al*. (1998)[160]	4	293 - 309	0.101325	0.032	0.009
Kiran & Sen (1992)[161]	47	323 - 448	8.0 - 66.5	1.6	1.4
Kumagai *et al*. (2006)[162]	16	273 - 334	0.1 - 30.0	0.053	0.043
Lampreia & Nieto de Castro (2011)[163]	117	283 - 324	0.1 - 60.0	0.026	0.025
Landaverde-Cortes *et al*. (2007)[92]	19	273 - 364	0.101325	0.033	0.004
Landolt & Jahn (1892)[164]	5	285 - 294	0.101325	0.16	0.11
Lei *et al*. (2010)[165]	8	283 - 319	0.101325	0.058	0.019
Lenoir *et al*. (1968)[166]	4	297.02	0.1 - 9.7	0.52	0.49
Ling & van Winkle (1958)[167]	4	303 - 369	0.101325	0.16	0.17
Liu & Zhu (2014)[168]	5	293 - 314	0.1	0.079	0.039
Liu *et al*. (2010)[104]	29	321 - 558	14.3 - 277	1.1	1.1
Lopez-Lazaro *et al*. (2015)[169]	7	293 - 324	0.101325	0.033	0.004
Lugo *et al*. (2001)[99]	81	278 - 354	0.1 - 25.0	0.052	0.02
Ma *et al*. (2004)[170]	10	313 - 394	0.1 - 6.1	0.34	0.33
Manzoni-Ansidei (1940)[171]	5	293 - 306	0.101325	0.076	0.034
Mascato *et al*. (2009)[172]	5	288 - 309	0.101325	0.037	0.006
Matos *et al*. (2001)[173]	5	283 - 314	0.101325	0.038	0.003
Moodley *et al*. (2018)[174]	126	313 - 364	0.1 - 20.1	0.12	0.076
Moore & Wellek (1974)[175]	4	293 - 314	0.101325	0.11	0.069
Moravkova *et al*. (2008)[176]	92	298 - 329	0.1 - 39.6	0.078	0.034
Moravkova *et al*. (2006)[177]	92	298 - 329	0.1 - 39.6	0.098	0.055
Moravkova & Linek (2008)[178]	4	298 - 329	0.101325	0.063	0.033
Moravkova & Linek (2003)[179]	20	298 - 329	2.1 - 38.6	0.092	0.049
Moravkova & Linek (2003)[180]	15	298 - 329	2.1 - 38.6	0.081	0.043
Mosteiro *et al*. (2009)[181]	5	288 - 309	0.101325	0.037	0.006
Navarro *et al*. (2016)[182]	8	278 - 339	0.101325	0.026	0.011
Ohji *et al*. (1999)[183]	4	283 - 329	0.101325	0.029	0.006
Orge *et al*. (1999)[184]	4	303 - 319	0.101325	0.031	0.006
Pardo *et al*. (2005)[185]	4	288 - 309	0.101325	0.03	0.013
Perez *et al*. (2016)[186]	5	283 - 329	0.1	0.04	0.015
Pimentel-Rodas *et al*. (2017)[187]	48	293 - 354	2.0 - 30.0	0.016	0.046
Pirdashti *et al*. (2020)[188]	6	288 - 314	0.1	0.035	0.007
Pugachevich & Cherkasskaya (1976)[189]	6	303 - 354	0.101325	0.054	0.034
Quayle *et al*. (1944)[190]	4	293 - 324	0.101325	0.029	0.011
Rama Rao (1940)[191]	6	273 - 324	0.101325	0.047	0.075
Ramos-Estrada *et al*. (2011)[192]	19	273 - 364	0.101325	0.019	0.028
Randova & Bartovska (2017)[193]	7	283 - 314	0.101325	0.013	0.047
Reyes-Garcia & Iglesias-Silva (2017)[93]	12	288 - 344	0.1	0.023	0.005
Rodriguez *et al*. (2003)[194]	4	293 - 314	0.101325	0.031	0.01
Rolling (1960)[195]	35	288 - 395	0.1 - 41.5	1.8	1.7
Sagdeev & Mukhamedzyanov (1977)[196]	55	273 - 373	<0.1 - 197	0.4	0.53
Sanmamed *et al*. (2009)[96]	117	283 - 324	0.1 - 60.0	0.049	0.012
Sato *et al*. (2010)[197]	4	323.2	0.2 - 10.4	0.23	0.22
Scaife & Lyons (1980)[198]	7	248 - 374	0.101325	0.06	0.076
Schedemann (2013)[98]	459	278 - 437	0.4 - 131	0.13	0.052
Schedemann (2009)[199]	459	283 - 443	0.3 - 130	0.11	0.13
Seyer & Gallaugher (1926)[200]	8	223 - 354	0.101325	0.68	0.68

Table 10: Continues on next page

Table 10 continued.

Reference	N	(T_{min} - T_{max}) / K	(p_{min} - p_{max}) / MPa	$AARD_{SW}$	$AARD_{This\ work}$
Shekaari *et al*. (2016)[201]	4	288 - 304	<0.1	0.097	0.053
Sperkach *et al*. (1979)[202]	7	223 - 324	0.101325	0.29	0.29
Takagi & Teranishi (1985)[203]	8	298 - 304	0.1 - 90.0	0.22	0.14
Tanaka *et al*. (1991)[204]	19	298 - 349	0.1 - 151	0.18	0.074
Tojo *et al*. (2004)[205]	5	293 - 319	0.101325	0.026	0.012
Trenzado *et al*. (2001)[206]	5	283 - 314	0.101325	0.025	0.018
Vogel (1946)[207]	9	293 - 360	0.101325	0.12	0.1
Watanabe & Moroto (1978)[208]	8	273 - 344	0.101325	0.18	0.15
Williams-Wynn *et al*. (2018)[209]	5	293 - 300	0.1	0.018	0.042
Wong & Hayduk (1990)[210]	21	298 - 349	0.1 - 6.9	0.23	0.25
Wu *et al*. (1998)[211]	4	293 - 314	0.101325	0.04	0.014
Yang *et al*. (2008)[212]	4	293 - 314	0.101325	0.031	0.01
Yang *et al*. (2004)[213]	7	298 - 354	0.101325	0.19	0.18
Yang *et al*. (2005)[214]	9	293 - 364	0.101325	0.21	0.2
Yu & Tsai (1995)[215]	5	293 - 314	0.101325	0.03	0.01
Yue *et al*. (2015)[216]	5	293 - 314	0.1	0.072	0.033

* Data were adopted from Gayol *et al*.[107]

[a] Dataset contains data in the critical and supercritical regions at low (LD), medium (MD), and high (HD) densities: $AARD_{LD} = 0.38$ %, $AARD_{MD} = 2.1$ %, $AARD_{HD} = 0.90$ %

[b] Dataset contains data in the supercritical region at medium (MD) and high (HD) densities: $AARD_{MD} = 2.6$ %, $AARD_{HD} = 0.29$ %

[c] Dataset contains data in the vapor (vap), liquid (liq), critical (crit), and supercritical region at low (LD), medium (MD), and high (HD) densities: $AARD_{vap} = 0.29$ %, $AARD_{liq} = 0.072$ %, $AARD_{crit} = 1.7$ %, $AARD_{LD} = 0.22$ %, $AARD_{MD} = 1.7$ %, $AARD_{HD} = 0.15$ %

3.5. Saturated densities

In addition to density data in the homogeneous region, densities in the saturated liquid and saturated vapor states were considered in the development of the new EOS. Figure 12 shows the percentage deviation of the available datasets and their corresponding AARD are given in Table 11. However, since densities at saturation are not independent properties but also affected by density data in the vicinity of the phase boundary, and information on the accuracy of the available saturated density data are very limited, only a small number of low-weighted data points along the saturated liquid curve were considered in the fitting process of the new EOS. Consequently, the course of the phase boundary is mainly dictated by selected homogeneous density and vapor-pressure data.

The available saturated liquid data cover almost the entire temperature range from the triple-point temperature to the critical temperature. Except for a few data points near the critical point and the dataset of McMicking and Kay,[44] all data points are reproduced within 0.3 %. The database for saturated vapor densities, on the other hand, is much more limited. Especially in the low temperature range ($T/T_c < 0.6$), only a few data points of low quality are available. The most comprehensive datasets, including data for both phases, were published by Young.[64,65] His first publication from 1900 comprises saturated liquid densities in a temperature range between 273 K and 564 K and saturated vapor densities between 393 K and 564 K. The results of that study were reevaluated and republished as part of a comprehensive project about the determination of vapor pressures, specific volumes, heats of vaporization, and critical constants of thirty pure substances in 1910. In both the saturated liquid and vapor phases, the revised results show higher consistency and lower scatter. However, while both datasets in the liquid phase are in good agreement with the new EOS and with data from Bagdasayan,[217] Badalyan *et al*.,[24] and Connolly and Kandalic,[29] their deviations significantly increase with decreasing temperature in the gas phase. Since none of the publications provide information about experimental uncertainties and sample purities, and the data of Badalyan *et al*.[24] and Connolly and Kandalic[29] contradict this trend at low temperatures, none of the data points were used to adjust the new EOS.

Badalyan *et al*.[24] determined vapor pressures and densities along the saturation curves in the medium and high temperature range. The authors stated uncertainties of 0.03 K in temperature, up to 0.08 % in liquid densities, and up to 0.2 % in vapor densities. Based on this information, combined uncertainties ($k = 2$) of 0.2 % for the liquid data and 0.4 % for the vapor data were determined, which increases near the critical temperature. However, since the data exhibit offsets and scatter in both phases that already exceed the estimated uncertainties, we assume that the experimental uncertainties are higher than those reported in the publication.

Based on the analysis of the available experimental database, the uncertainty of the new EOS is estimated to be 0.3 % in the saturated liquid phase. However, due to the accurate description of homogeneous liquid densities near the phase boundary and the available vapor-pressure data (see Secs. 3.4 and 3.2), we estimate the uncertainty in the saturated liquid phase to be 0.2 % for temperatures below 440 K. The limited data quality and quantity in the saturated vapor phase does not allow for a reasonable uncertainty estimation.

Table 11. AARD of saturated density data calculated with the new EOS and the EOS of Span and Wagner.[2] AARD are given for the low (LT: $T/T_c < 0.6$), medium (MT: $0.6 \leq T/T_c \leq 0.98$), and high (HT: $T/T_c > 0.98$) temperature ranges as well as the overall values.

			$AARD_{SW}$				$AARD_{This\ work}$			
Reference	N	(T_{min} - T_{max}) / K	LT	MT	HT	Overall	LT	MT	HT	Overall
Saturated liquid density ρ'										
Aminabhavi & Banerjee (2001)[218]	3	298 - 309	0.18	...	...	0.18	0.14	...	...	0.14
Badalyan *et al*. (1986)[24]	22	423 - 569	...	0.45	4.3	2.2	...	0.12	0.83	0.44
Bagdasayan (1964)[217]	8	243 - 393	0.054	0.24	...	0.13	0.045	0.16	...	0.088
Connolly & Kandalic (1962)[29]	11	463 - 554	...	0.45	...	0.45	...	0.054	...	0.054
Dymond & Young (1980)[219]	3	298 - 334	0.098	...	...	0.098	0.071	...	...	0.071
Kumar *et al*. (1994)[220]	1	303.15	0.044	...	...	0.044	0.003	...	...	0.003
McMicking & Kay (1965)[44]	17	403 - 564	...	0.26	1.7	0.34	...	0.64	0.6	0.64
Meeussen *et al*. (1967)[221]	3	298 - 329	0.071	...	...	0.071	0.092	...	...	0.092
Rozhnov (1967)[54]	4	303 - 414	0.01	0.1	...	0.078	0.031	0.016	...	0.02
Terry *et al*. (1960)[222]	1	298.14	0.044	...	...	0.044	0.0002	...	...	0.0002
Young (1900)[65]	28	273 - 564	0.071	0.25	3.3	0.33	0.084	0.11	1.1	0.14
Young (1910)[64]	30	273 - 564	0.015	0.24	3	0.28	0.036	0.13	0.74	0.13
Saturated vapor density ρ''										
Badalyan *et al*. (1986)[24]	17	423 - 569	...	0.86	6.2	4.3	...	0.79	1.2	1.1
Connolly & Kandalic (1962)[29]	10	463 - 554	...	0.52	...	0.52	...	0.3	...	0.3
Lee *et al*. (2009)[223]	2	333 - 354	3.3	0.26	...	1.8	3.7	0.022	...	1.9
McMicking & Kay (1965)[44]	7	503 - 564	...	4.4	3.6	4.3	...	4.7	0.38	4.1
Rozhnov (1967)[54]	4	303 - 414	11	4.3	...	6	12	4.4	...	6.4
Young (1900)[65]	20	393 - 554	...	1.3	...	1.3	...	1.3	...	1.3
Young (1910)[64]	18	393 - 564	...	0.93	3.9	1.1	...	0.74	0.68	0.74

3.6. Thermal virial coefficients

The available experimental data of the second thermal virial coefficient B and third thermal virial coefficient C are summarized in Table 12 and illustrated in Fig. 13. Due to the zero crossing of both virial coefficients, their steep slopes, and high magnitudes at low temperatures, the average absolute relative deviation (AARD) is less meaningful for validation and could lead to false conclusions. Therefore, average absolute deviations (AAD) are given in Table 12 instead of relative deviations.

The database for *n*-octane comprises virial coefficients obtained by direct measurement techniques and theoretical approaches as well as data derived from homogeneous gas properties. The most common approach for the determination of virial coefficient data from homogeneous gas properties data is the use of virial EOS, which are usually truncated after the second or third coefficient. Consequently, the resulting virial coefficients are not an independent property but depend on the property they are derived from and, therefore, redundant if the EOS is fitted to the underlying homogeneous gas data. Conversely, virial coefficient data have to be consistent with fitted homogeneous gas data to be reproduced within their experimental uncertainty. The new EOS was fitted to gas density data of Badalyan *et al*.[88] and isobaric heat capacity data of Hossenlopp and Scott.[13] Since some second virial coefficient datasets show contradictory trends, and attempts to include virial coefficient data in the fitting process resulted in lower accuracies in other gas-phase properties, the new EOS was not fitted to virial coefficient data. Therefore, data of the second and third viral coefficient were solely used for validation. For a meaningful validation of the thermal virial coefficients, an evaluation of the gas property from which the virial coefficients were derived can provide important information about the data quality. However, the most comprehensive dataset provided by Millat *et al*.[46] does not include the original experimental data but only fitted virial coefficients. Millat *et al*.[46] determined densities in a temperature range from 397 K to 575 K with a quasi-isochoric measuring method, from which the authors derived the second thermal virial coefficients. To evaluate a truncated virial equation, the authors used three different methods, which are explained in more detail in the corresponding publication. The maximum uncertainty is assumed to be 3 % for all three approaches, corresponding to absolute uncertainties between 20 $cm^3\ mol^{-1}$ and 55 $cm^3\ mol^{-1}$. Except for three data points calculated with the first evaluation scheme, all data points are represented within their uncertainties. In the temperature range from 337 K to 426 K, Hossenlopp and Scott[13] provide second virial coefficients obtained by the use of the Clapeyron equation and experimentally determined enthalpies of vaporization. The stated uncertainty decreases from 780 $cm^3\ mol^{-1}$ to 6 $cm^3\ mol^{-1}$ with increasing temperature. Six of the nine data points are reproduced within their corresponding uncertainty by the new EOS. However, since the new EOS is able to reproduce the enthalpies of vaporization within their experimental uncertainty of less than 0.1 % (see Sec. 3.3), we assume that the uncertainty estimation of Hossenlopp and Scott[13] for the second virial coefficients was too optimistic. Overall, the new EOS reproduces the data of Hossenlopp and Scott[13] with an AAD of 25 $cm^3\ mol^{-1}$.

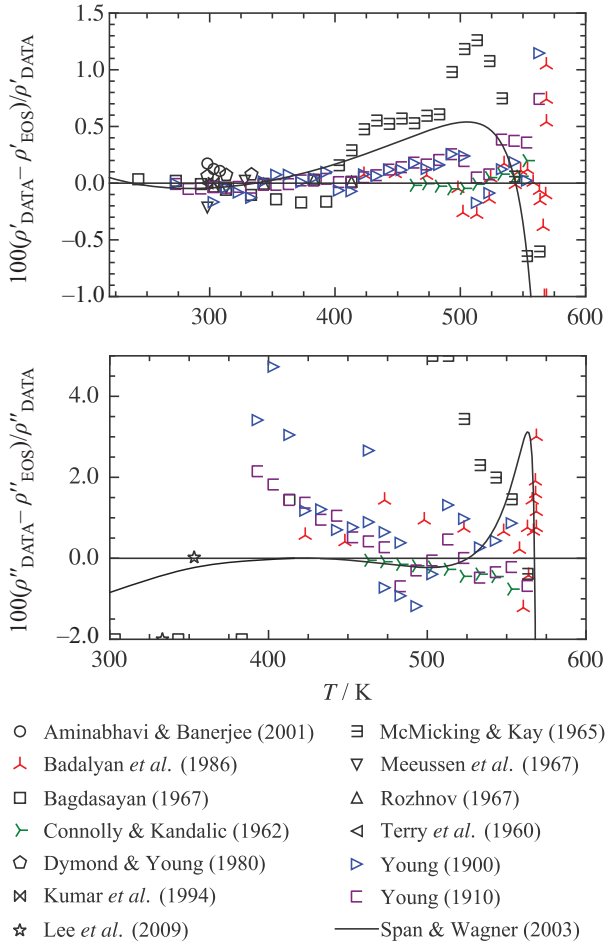

Figure 12. Percentage deviation of saturated liquid (top) and saturated vapor (bottom) density data from the new EOS and the EOS of Span and Wagner.[2]

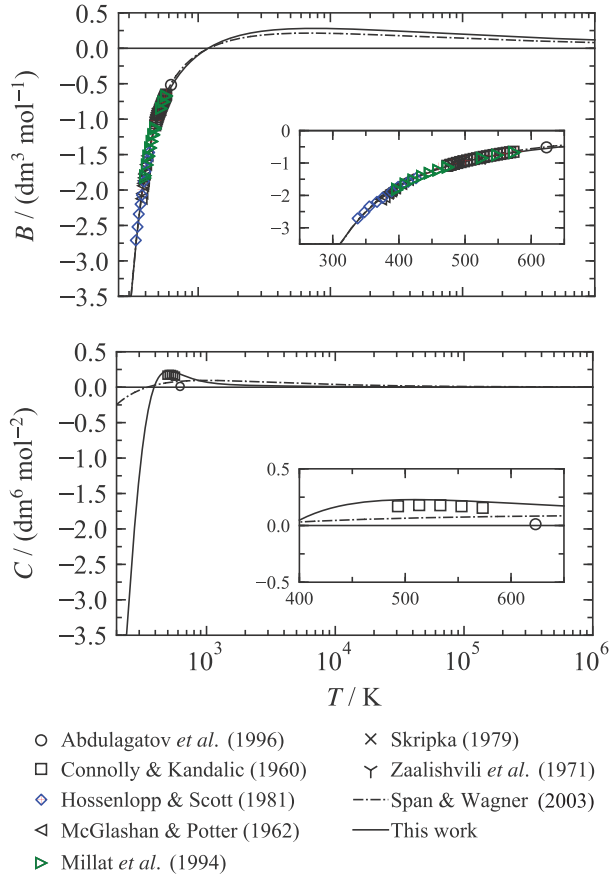

Figure 13. Second virial coefficient B (top) and third virial coefficient C (bottom) as a function of temperature calculated with the new EOS and the EOS of Span and Wagner.[2]

In addition to the reproduction of the data, the course of virial coefficients with temperature is an important criterion for the evaluation of the physical behavior of an EOS. The focus in developing the new EOS was initially to obtain the correct behavior and secondly to combine it with an acceptable reproduction of the available literature data. As shown in the top panel of Fig. 13, both the EOS of Span and Wagner[2] and the new EOS agree with the experimental data, which show large negative virial coefficients, a positive slope, and negative curvature. With increasing temperature, both EOS exhibit the correct behavior indicated by crossing the zero line, followed by a maximum, and approaching zero again without becoming negative. The same criteria are valid for the behavior of the third thermal virial coefficient (see Fig. 13 bottom panel), except that the maximum should be more distinct. Only a dataset of Connolly and Kandalic[224] and a single data point of Abdulagatov *et al*.[89] are available for quantitative validation. Qualitatively, both EOS show the correct behavior at high temperatures. In the low-temperature region, however, the EOS of Span and Wagner[2] exhibits a low slope and, thus, a qualitatively incorrect behavior.

3.7. Isobaric thermal expansivity, isothermal and isentropic compressibility

Although data for the isobaric thermal expansivity α_v, isothermal compressibility κ_T, and isentropic compressibility κ_s were not considered in the fitting process of the new EOS, they were used for additional evaluations. According to Eqs. (17) to (19), they describe the pressure and temperature dependence of density and thus represent the slope of isobars, isotherms, and isentropes in corresponding density diagrams.

$$\alpha_v = \frac{1}{v}\left(\frac{\partial v}{\partial T}\right)_p \tag{17}$$

$$\kappa_T = -\frac{1}{v}\left(\frac{\partial v}{\partial p}\right)_T \tag{18}$$

$$\kappa_s = \frac{1}{v}\left(\frac{\partial v}{\partial T}\right)_s \tag{19}$$

The correct description of these properties alone is not an indicator for the correct description of the homogeneous density, as a systematically offset EOS can also exhibit a correct

Table 12. AADs of virial coefficient data calculated with the new EOS and the EOS of Span and Wagner.[2]

Reference	N	(T_{min} - T_{max}) / K	AAD_{SW}	$AAD_{This\ work}$
	Second virial coefficient B ($cm^3\ mol^{-1}$)			
Abdulagatov *et al*. (1996)[89]	1	623.15	16	30
Connolly & Kandalic (1960)[224]	21	473 - 574	19	21
Hossenlopp & Scott (1981)[13]	9	337 - 426	35	25
McGlashan & Potter (1962)[225]	10	372 - 414	21	28
Millat *et al*. (1994)[46]	30	397 - 575	58	28
Skripka (1979)[226]	1	523.11	66	26
Zaalishvili *et al*. (1971)[227]	5	478 - 499	23	59
	Third virial coefficient C ($cm^6\ mol^{-2}$)			
Abdulagatov *et al*. (1996)[89]	1	623.15	72	174
Connolly & Kandalic (1960)[224]	5	493 - 574	100	51

slope. Consequently, the isobaric thermal expansivity, isothermal compressibility, and isentropic compressibility have to be evaluated along with homogeneous density data. The relative deviations of the available datasets to the new EOS and the EOS of Span and Wagner[2] are illustrated in Fig. 14 and their corresponding AARD are given in Table 13.

Except for the dataset of Navia *et al*.,[228] all available data of the isobaric thermal expansivity were measured at atmospheric pressure. To determine data in a temperature range from 248 K to 349 K at pressures up to 55 MPa, Navia *et al*.[228] used a twin cell microcalorimeter. Considering heat leaks of up to 10 % due to pressure variations, the combined uncertainty was estimated by the authors to be 2 %. Only a single data point exceeds the stated uncertainty with a deviation of 2.4 %. Overall, the dataset is reproduced with an AARD of 0.56 %. At atmospheric pressure, the most comprehensive dataset is provided by Cerdeiriña *et al*.[91] To obtain isobaric thermal expansivity values from experimentally determined density data, the authors numerically evaluated the change in density in a temperature interval of 10 K. The uncertainty in the obtained isobaric thermal expansivity is estimated to be 3×10^{-6} K^{-1}. Considering an uncertainty of 0.01 K in temperature, a combined uncertainty ($k = 2$) ranging from 0.48 % to 0.53% was calculated by applying Gaussian error propagation. Only a single data point exceeds the uncertainty by 0.05%. The AARD of the dataset from the new EOS is 0.18%. In addition to isobaric thermal expansivities, the authors calculated isentropic compressibility data by combining their experimentally determined densities and speeds of sound with the Laplace equation. An estimated uncertainty of 0.15 TPa^{-1} leads to a combined uncertainty ($k = 2$) between 0.028 % and 0.035 %. Except for a few data points, which exceed their combined uncertainty by 0.001 - 0.002 %, the EOS reproduces all data within their uncertainty with an AARD of 0.016 %. Since Cerdeiriña *et al*.[91] also measured isobaric heat capacities with a second experimental setup, the authors combined all their results by calculating the isothermal compressibility. Based on the uncertainties of each property, the uncertainty of isothermal compressibilities was estimated as 1 TPa^{-1}, resulting in a maximum relative uncertainty ($k = 2$) of 0.17 %. The new EOS describes 98 % of the data within their uncertainties with an AARD of 0.059 %. In the pressure range above ambient pressure, two datasets of Moravkova *et al*.[176,177] are available. In both publications, the authors fitted a Tait equation to their experimentally determined density data in order to obtain the pressure derivative of density at constant temperature, which is required for the calculation of isothermal compressibilites. While the primary density datasets are well reproduced by the new EOS (cf. Table 10), the calculated isothermal compressibilites deviate by up to 8 % and exhibit contradictory trends. Therefore, we conclude an insufficient description of the density data by the fitted Tait equation. To verify this assumption, we replaced the derivative of the Tait equation with a derivative of the new EOS and recalculated the isothermal compressibilites based on the experimental densities, even though the results of this approach are no longer independent of the EOS and, therefore, have less significance. By changing the derivatives, the AARD can be reduced from 3.5 % and 2.4 % to 0.035 % and 0.055 %.

3.8. Speed of sound

With 1114 data points, speed of sound is the second largest database of all available properties for *n*-octane. The homogeneous liquid phase in a temperature range from 218 K to 643 K with pressures up to 300 MPa as well as the saturated liquid and saturated vapor phase are covered. However, only 13 of 45 available datasets comprise data at pressures above atmospheric pressure. The calculated AARD of each dataset is given in Table 14, including their corresponding temperature and pressure ranges. Deviation diagrams of all available data divided into isotherms are provided in the supplementary material.

Figure 15 shows the percentage deviation of the new EOS to datasets at ambient pressure with more than three data points and the EOS of Span and Wagner.[2] At atmospheric pressure, the new EOS was fitted to the experimental data of Cerdeiriña *et al*.[91] As discussed in Sec. 3.4, the authors used a combined instrument to determine density and speed of sound data simultaneously. With an ultrasonic pulse analysis, 46 speed of sound data points were obtained in a temperature range between 288 K and 334 K. Therefore, it is the most comprehensive dataset in terms of number of data points of all available atmospheric datasets. The accuracy of temperature and

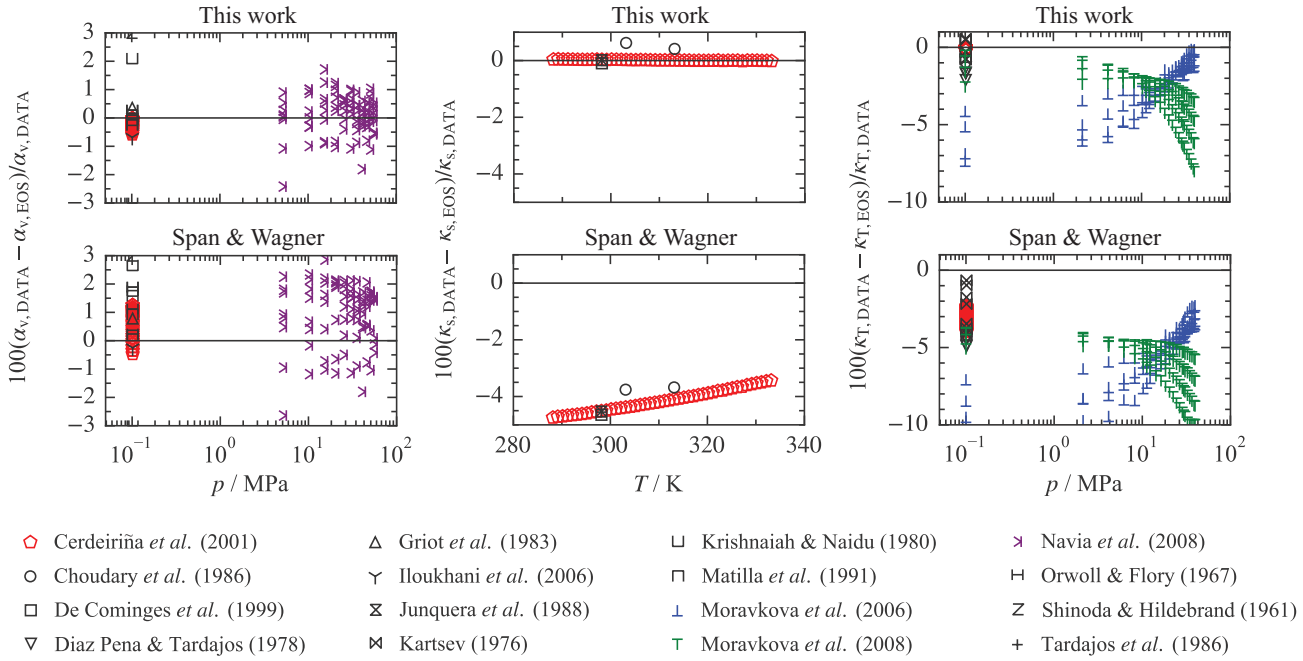

Figure 14. Percentage deviation of isobaric thermal expansivity (left), isothermal compressibility (center), and isentropic compressibility (right) data from the new EOS (top) and the EOS of Span and Wagner[2] (bottom).

Table 13. AARD of isobaric thermal expansivity, isothermal compressibility, and isentropic compressibility data calculated with the new EOS and the EOS of Span and Wagner.[2]

Reference	N	(T_{min} - T_{max}) / K	(p_{min} - p_{max}) / MPa	$AARD_{SW}$	$AARD_{This\ work}$
		Isobaric thermal expansivity α_v			
Cerdeiriña *et al.* (2001)[91]	46	288 - 334	0.101325	0.66	0.18
Griot *et al.* (1983)[229]	1	298.14	0.101325	0.78	0.36
Iloukhani *et al.* (2006)[230]	1	298.15	0.101325	0.25	0.68
Krishnaiah & Naidu (1980)[231]	1	303.14	0.101325	2.7	2.1
Matilla *et al.* (1991)[232]	2	298 - 319	0.101325	0.55	0.15
Navia *et al.* (2008)[228]	88	278 - 349	5.1 - 54.6	1.3	0.56
Orwoll & Flory (1967)[233]	7	293 - 414	0.101325	1.4	0.26
Shinoda & Hildebrand (1961)[234]	1	298.14	0.101325	15	14
Tardajos *et al.* (1986)[235]	1	298.14	0.101325	0.61	0.19
		Isentropic compressibility κ_s			
Cerdeiriña *et al.* (2001)[91]	46	288 - 334	0.101325	4.1	0.016
Choudary *et al.* (1986)[236]	2	303 - 314	0.101325	3.7	0.52
De Cominges *et al.* (1999)[237]	1	298.15	0.101325	4.6	0.097
Junquera *et al.* (1988)[238]	1	298.14	0.101325	4.5	0.014
Tardajos *et al.* (1986)[235]	1	298.14	0.101325	4.6	0.006
		Isothermal compressibility κ_T			
Cerdeiriña *et al.* (2001)[91]	46	288 - 334	0.101325	3.1	0.059
Diaz Pena & Tardajos (1978)[129]	4	298 - 334	0.101325	4.7	1.7
Kartsev (1976)[239]	8	293 - 364	0.101325	2.6	0.55
Moravkova *et al.* (2008)[176]	92	298 - 329	0.1 - 39.6	6.3	3.5
Moravkova *et al.* (2006)[177]	92	298 - 329	0.1 - 39.6	5.1	2.4

speed of sound measurements was estimated to 0.01 K and 1 m s^{-1}, corresponding to a combined relative uncertainty ($k = 2$) of 0.033 %. The highly consistent data are reproduced by the new EOS within their experimental uncertainty with an AARD of 0.007 % and a maximum deviation of 0.018 %. The results of Cerdeiriña *et al.*[91] are confirmed by the data of Devi *et al.*[128] Furthermore, the datasets of Jin *et al.*,[240] Kashyap *et al.*,[241] and Rodriguez *et al.*,[242] which are not illustrated in Fig. 15 due to their small number of data points, are in good agreement.

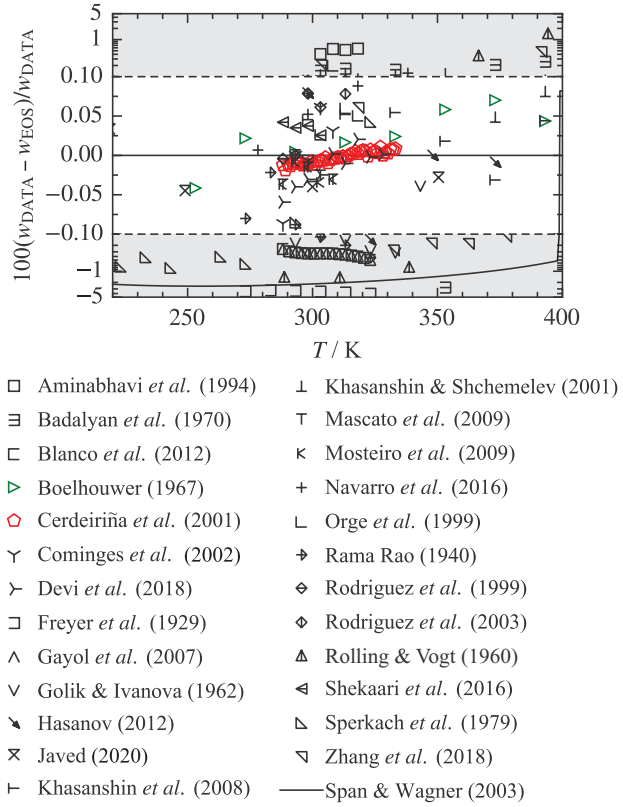

Figure 15. Percentage deviation of selected speed of sound data at atmospheric pressure from the new EOS and the EOS of Span and Wagner.[2] The ordinate is linearly scaled between the dashed lines and logarithmically scaled in the gray filled regions.

Outside the temperature range of the dataset of Cerdeiriña *et al.*,[91] few data are available. One of the most consistent datasets covering a wide temperature range is provided by Boelhouwer,[243] who measured speed of sound data over a wide temperature and pressure range with a pulse-echo method with constant path length. Although the author does not provide a detailed uncertainty analysis, the total uncertainty is stated to be 0.1 %. However, it is not specified whether this a standard or expanded uncertainty. Furthermore, it is unknown if the sample purity of 99.6 mol % is considered in the uncertainty analysis. The eight data points at ambient pressure deviate with an AARD of 0.035 %.

At elevated pressures, the new EOS was adjusted to the dataset of Javed.[244] The author measured seven isotherms over a temperature range between 219 K and 500 K with pressures up to 125 MPa using a double path length pulse-echo technique. Considering the standard uncertainties for temperature, pressure, delay in time of flight, and path length difference measurements, the overall expanded uncertainty ($k = 2$) of each state point ranges from 0.011 % to 0.050 %. Overall, the dataset is reproduced with an AARD of 0.044 % by the new EOS. Although the majority of the data is reproduced slightly above (0.02 %) their specified experimental uncertainty, the deviation is estimated to be correct because the sample purity of >99 mol% is not considered in the experimental uncertainty budget. Selected isotherms of the dataset are shown in Fig. 16.

The results of Javed[244] are confirmed by measurements of Khasanshin *et al.*[245] and Badalyan *et al.*[246] The measurements of Khasanshin *et al.*[245] extend over a temperature range from 298 K to 434 K at pressures up to 101 MPa. Uncertainties in temperature, pressure, and speed of sound are given as 0.02 K, 0.05 %, and 0.1 %. Applying Gaussian error propagation, a combined uncertainty of 0.2 % ($k = 2$) was determined. Except for one data point, all data points are represented within their specified uncertainties. Badalyan *et al.*[246] used an ultrasonic pulse-echo method for measurements in a temperature range between 304 K and 394 K and pressures up to 118 MPa. The experimental uncertainty is given as 0.2 % in the Russian publication. The entire dataset is reproduced with an AARD of 0.18 %. However, two data points deviate significantly more with errors of 2.8 % and 1.3 %. The first point was measured at atmospheric pressure and 353 K, while the second data point was measured at 117 MPa and 373 K. Due to the different location of the data points, we assume a non-systematic measurement error. When these two points are neglected in the calculation, the AARD is reduced to 0.13 %.

The most comprehensive dataset in terms of number of data points is provided by Zhang *et al.*[247] 257 data points along five isobars in the homogeneous liquid and six isobars in the supercritical region with pressures up to 12 MPa were determined using the Brillouin light scattering method with an estimated expanded uncertainty ($k = 2$) of 1.3 %. Because the dataset was not available until the adjustment process of the new EOS was completed, the data were not considered in the fitting process but solely for validation. As shown in Fig. 17, the data at temperatures above 360 K exhibit a large scatter and a systematic offset to the datasets of Badalyan *et al.*,[246] Boelhouwer,[243] Javed,[244] and Khasanshin *et al.*[245] Nevertheless, the majority of the data in the subcritical temperature region are reproduced within their uncertainty with an AARD of 0.88 %. Only the 4 MPa isobar shows a significantly higher deviation of up to 9 % in the subcritical temperature region. As illustrated in Fig. 18, data along this isobar exhibit a strong unreasonable change in curvature between 550 K and 570 K resulting in a high deviation. In the supercritical temperature region, a systemic offset beginning at about 600 K is present, exemplified by the 6 MPa and 7 MPa isobars in Fig. 18. Due to the high scatter and systematic offset, we conclude that the uncertainties were estimated too optimistically. Therefore, the dataset is not used for uncertainty estimates of the EOS, although no other data are available in the high-temperature region.

In addition to data in the homogeneous region, speed of sound data along the saturation curves were considered in the fitting process of the new EOS. Figure 19 shows the speed of sound as a function of temperature calculated with the new EOS and the available saturation datasets of Neruchev,[248] Neruchev *et al.*,[249] and Zotov *et al.*[250] The three available experimental datasets were all measured by the same research group and are in good agreement with the new EOS over the entire temperature range (cf. Fig. 20). Neruchev *et al.*[249] carried out measurements in the saturated liquid phase with an estimated uncertainty of 2 m s^{-1}, corresponding to a

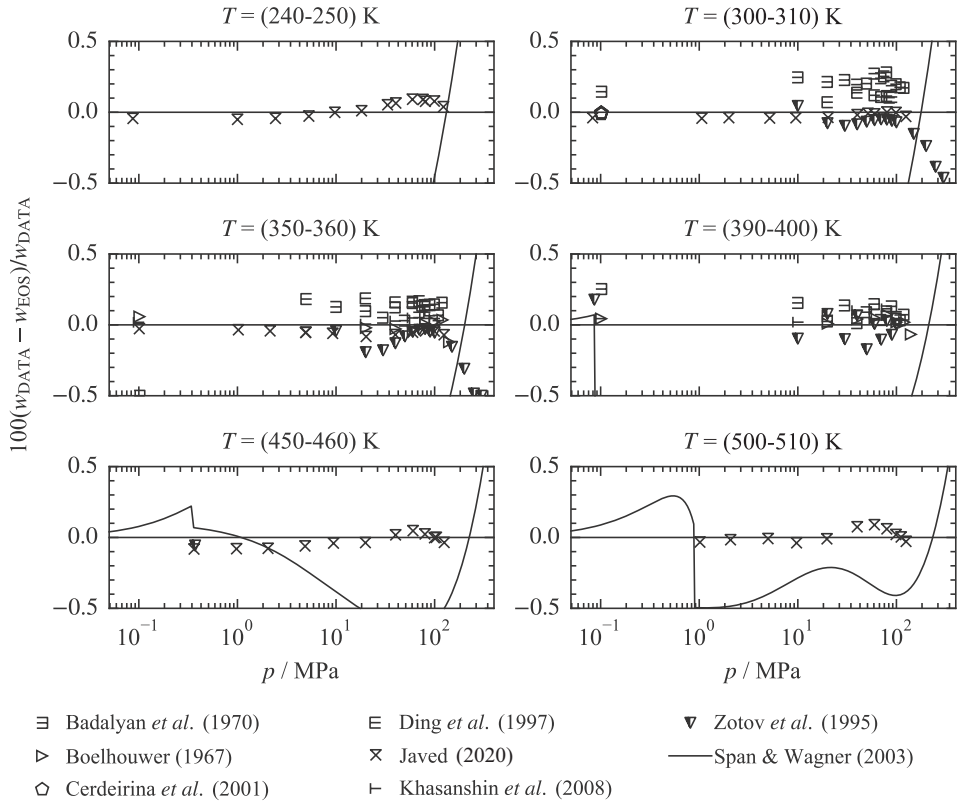

Figure 16. Percentage deviation of speed of sound data at selected isotherms in the liquid phase from the new EOS and the EOS of Span and Wagner.[2]

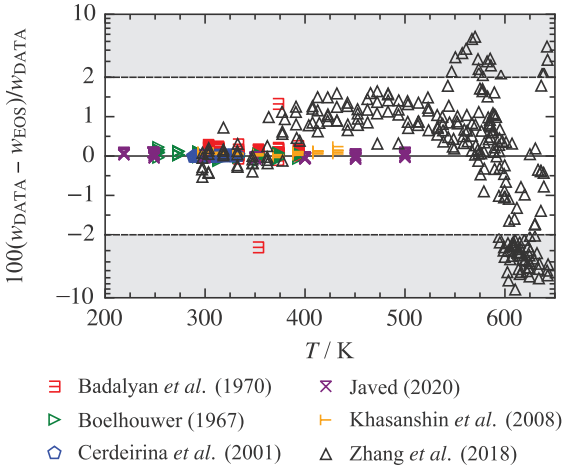

Figure 17. Percentage deviation of selected speed of sound data from the new EOS. The ordinate is linearly scaled between the dashed lines and logarithmically scaled in the gray filled regions.

relative uncertainty between 0.14 % and 2.7 %. The new EOS describes all data within the experimental uncertainty with an overall AARD of 0.53 %. In the same year, Neruchev[248] published a dataset comprised of speed of sound data at the saturated liquid and vapor phases. However, no detailed statement about the experimental uncertainty of the data could be obtained from the corresponding Russian publication. Furthermore, the dataset includes 5 data points at supercritical temperatures (cf. Fig. 19), which are neglected in the evaluation. Assuming an identical uncertainty of 2 m s^{-1} as given in Neruchev *et al.*,[249] the data are reproduced within their uncertainty with an AARD of 0.75 % in the saturated liquid phase and 0.30 % in the saturated vapor phase. The dataset of Zotov *et al.*[250] comprises data at both saturation states as well as data in the homogeneous liquid region. However, no information about the measurement technique and its accuracy was available to us. While the 80 data points in the homogeneous liquid phase are reproduced with an AARD of 0.16 %, the deviation of the saturated data is about two times higher with 0.37 % and 0.34 %.

In the vicinity of the critical point, both the available data and the EOS show a decrease in speed of sound and indicate a global minimum consistent with the theory of a speed of sound limit of zero at the critical point. Even though the relative deviation of the EOS increases up to 2 % near the critical point (cf. Figure 20) and it does not reach the theoretical limiting value, the formation of a global minimum where the saturated liquid and vapor lines meet is an important criterion to describe the critical region.

To compare the new EOS with the EOS of Span and Wagner[2] in regions where no experimental data are available, the percentage deviation in speed of sound between both mod-

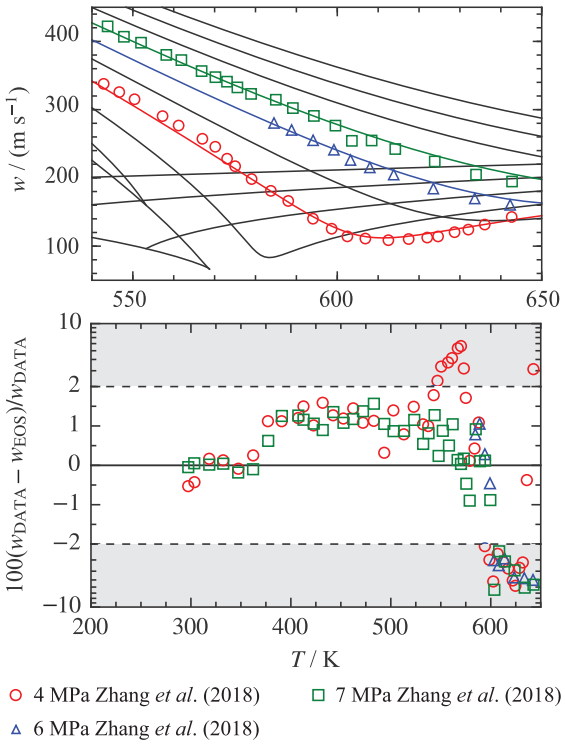

Figure 18. w,T-diagram (top) and percentage deviation (bottom) of selected speed of sound data of Zhang *et al*.[247] from the new EOS. The ordinate is linearly scaled between the dashed lines and logarithmically scaled in the gray filled regions.

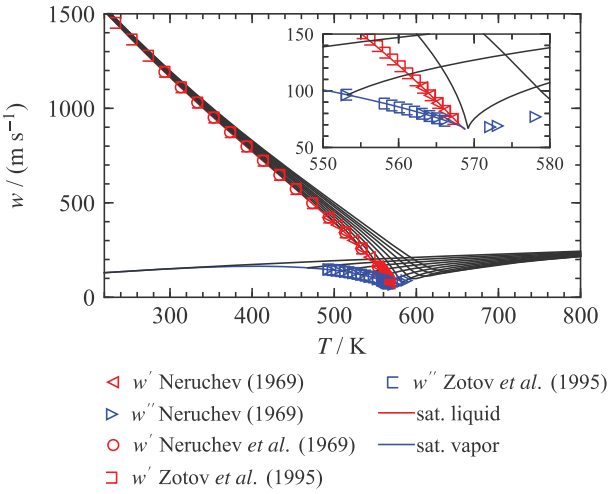

Figure 19. w,T-diagram calculated with the new EOS at pressures up to 5 MPa showing saturated speed of sound data.

els is illustrated over a wide temperature and pressure range in Fig. 21. The highest deviations of up to 3 % are located in the liquid phase at temperatures below 400 K, in the vicinity of the critical point, and at pressures above 500 MPa. While the deviation in the liquid phase and in the vicinity of the critical point are attributable to fitted experimental data and different critical properties, the deviation in the high-pressure

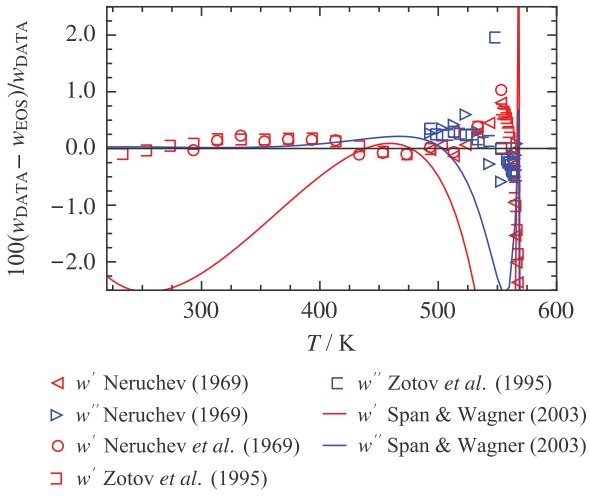

Figure 20. Percentage deviation of speed of sound data in the saturated liquid and saturated vapor phases from the new EOS and the EOS of Span and Wagner.[2]

region results from different extrapolation behaviors of the EOS. However, since no experimental data are available in the high-pressure region, the models cannot be validated. Although none of the models were fitted to experimental speed of sound data in the vapor phase, the deviation between the models in this region is comparatively small. This similar behavior of the EOS is related to a nearly identical description of the available isobaric heat capacity data in the vapor phase (see Sec. 3.9) and the close mathematical correlation between these properties. Both properties are formulated by the same terms and derivatives of the Helmholtz energy and are, therefore, strongly correlated.

Based on the description of the experimental database, the uncertainty in speed of sound of the new EOS was estimated as a function of temperature and pressure as shown in Fig. 22. Since no experimental data are available in the vapor phase and supercritical region, no uncertainties could be estimated in these state regions. At very low densities, however, the vapor approaches the ideal-gas state and, thus, the uncertainty in speed of sound correlates with the accuracy of the ideal-gas heat capacity. At the lower temperature end, the range of validity is bordered by the solid phase.

3.9. Heat capacities

An overview of the available experimental database for isobaric and isochoric heat capacities including their deviations to values calculated from the new EOS and the EOS of Span and Wagner[2] is given in Table 15. Although the number of available publications is relatively high, only small parts of the state region are covered by experimental data, since the majority of the publications merely provide data at atmospheric pressure. Furthermore, about half of the available publications include only a single experimental data point. The deviations of isobaric heat capacity datasets at atmospheric pressure with more than one data point are illustrated in Fig. 23. In the liquid

Table 14. AARD of speed of sound data calculated with the new EOS and the EOS of Span and Wagner.[2]

Reference	N	(T_{min} - T_{max}) / K	(p_{min} - p_{max}) / MPa	$AARD_{SW}$	$AARD_{This\ work}$
Aminabhavi *et al*. (1994)[112]	5	298 - 319	0.101325	2.4	0.41
Badalyan *et al*. (1970)[246]	78	303 - 394	0.1 - 118	1.3	0.18
Blanco *et al*. (2012)[251]	15	288 - 324	0.101325	1.7	0.35
Boelhouwer (1967)[243]	64	253 - 394	0.1 - 141	1.1	0.057
Cerdeiriña *et al*. (2001)[91]	46	288 - 334	0.101325	2	0.007
Cholpan *et al*. (1981)[252]	3	253 - 344	0.101325	1.5	0.56
Cominges *et al*. (2002)[126]	5	288 - 309	0.101325	2.2	0.037
Devi *et al*. (2018)[128]	9	288 - 329	0.101325	2	0.021
Ding *et al*. (1997)[253]	71	293 - 364	5.0 - 90.0	1.4	0.11
Dubey & Sharma (2008)[254]	3	298 - 309	0.101325	2.2	0.072
Freyer *et al*. (1929)[141]	6	273 - 324	0.101325	1.4	3.6
Gayol *et al*. (2007)[107]	15	288 - 324	0.101325	1.7	0.35
Golik & Ivanova (1962)[255]	6	293 - 344	0.101325	1.7	0.18
Gonzalez *et al*. (2003)[256]	3	293 - 304	0.101325	2.2	0.047
Hasanov (2012)[257]	74	298 - 524	0.1 - 58.9	1.4	0.83
Javed (2020)[244]	77	218 - 501	<0.1 - 126	1.1	0.044
Jin *et al*. (2019)[240]	3	298 - 319	0.1	2	0.018
Kashyap *et al*. (2018)[258]	3	293 - 304	0.101325	2.1	0.038
Kashyap *et al*. (2020)[241]	3	298 - 319	0.101325	2	0.018
Khasanshin & Shchemelev (2001)[259]	46	303 - 434	0.1 - 49.1	1.4	0.092
Khasanshin *et al*. (2008)[245]	49	298 - 434	0.1 - 101	1.2	0.071
Mascato *et al*. (2009)[172]	5	288 - 309	0.101325	2.2	0.022
Mosteiro *et al*. (2009)[181]	5	288 - 309	0.101325	2.1	0.025
Navarro *et al*. (2016)[182]	4	278 - 339	0.101325	2.1	0.068
Nayeem *et al*. (2016)[260]	3	308 - 319	0.101325	2.5	0.52
Neruchev (1969)[249]	23	493 - 589	0.8 - 2.4	1.8	0.53[a]
Neruchev *et al*. (1969)[248]	14	293 - 554	<0.1 - 2.0	1.5	0.2
Orge *et al*. (1999)[184]	4	303 - 319	0.101325	2.1	0.084
Oswal *et al*. (2004)[261]	3	298 - 314	0.101325	2.2	0.095
Rama Rao (1940)[191]	6	273 - 324	0.101325	2	0.16
Rathnam *et al*. (2010)[262]	3	303 - 314	0.101325	2	0.19
Rodriguez *et al*. (1999)[242]	3	288 - 299	0.101325	2.3	0.028
Rodriguez *et al*. (2003)[194]	4	293 - 314	0.101325	2.2	0.055
Rolling & Vogt (1960)[195]	30	288 - 395	0.1 - 34.6	1.9	3.3
Shekaari *et al*. (2016)[201]	4	288 - 304	<0.1	2.2	0.035
Sperkach *et al*. (1979)[202]	7	223 - 324	0.101325	1.9	0.45
Takagi & Teranishi (1985)[203]	3	298.14	0.1 - 100	1.9	0.39
Zhang *et al*. (2018)[247]	257	296 - 644	0.1 - 12.0	2.1	1.5[b]
Zotov *et al*. (1995)[250]	134	233 - 568	<0.1 - 300	1.6	0.24[c]

[a] dataset contains data in the saturated vapor (sat.vap) and saturated liquid (sat.liq) phases:
$AARD_{sat.vap} = 0.30$ %, $AARD_{sat.liq} = 0.75$ %
[b] dataset contains data in the homogeneous liquid (liq), critical (crit), and supercritical region at low (LD), medium (MD), and high (HD) densities:
$AARD_{liq} = 0.88$ %, $AARD_{crit} = 2.3$ %, $AARD_{LD} = 1.5$ %, $AARD_{MD} = 3.1$ %, $AARD_{HD} = 1.5$ %
[c] dataset contains data in the homogeneous liquid (liq), saturated vapor (sat.vap), and saturated liquid phases (sat.liq):
$AARD_{liq} = 0.16$ %, $AARD_{sat.vap} = 0.35$ %, $AARD_{sat.liq} = 0.37$ %

phase, the new EOS was fitted to the dataset of Cerdeiriña *et al*.[91] The authors performed highly accurate measurements at atmospheric pressure by using differential scanning calorimetry. The accuracy is estimated to be 0.15 J mol^{-1}K^{-1} corresponding to a relative uncertainty of 0.058 %. Although the estimated uncertainty seems to be very optimistic, the EOS describes all data points with a maximum deviation of 0.037 % and, therefore, within their reported uncertainty. Outside the temperature range of Cerdeiriña *et al*.,[91] only Ayurov *et al*.[263] provide data of comparable quality. As shown in Fig. 23, most of the available datasets exhibit high scatter and contradictory trends, and are, therefore, not appropriate for validation. However, in the overlapping temperature range, the results of Ayurov *et al*.[263] confirm the data of Cerdeiriña *et al*.[91] While the deviation of the data of Ayurov *et al*.[263] remains in the same order of magnitude down to temperatures of 223 K, it increases up to 1 % with increasing temperature. Even though this deviation is still within the reported experimental uncertainty of up to 2.5%, it cannot be ruled out that evaporation of the sample has already occurred at the high-

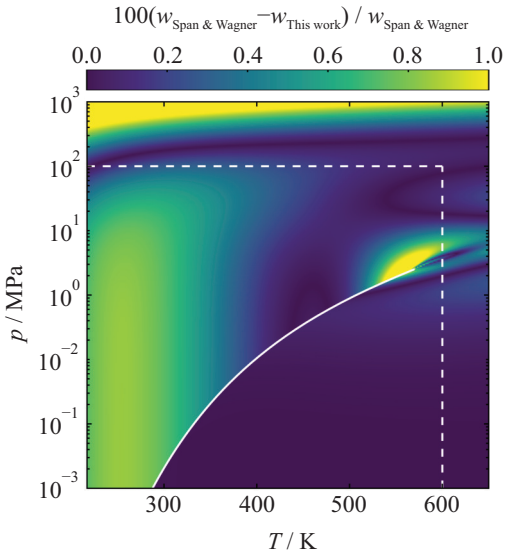

Figure 21. Percentage deviation in speed of sound in the homogeneous region between the new EOS and the EOS of Span and Wagner.[2] The white dashed lines mark the normal range of validity of the model by Span and Wagner,[2] whereas the range of the new model corresponds to the axis limits. The solid white curve represents the vapor-pressure curve of the new model.

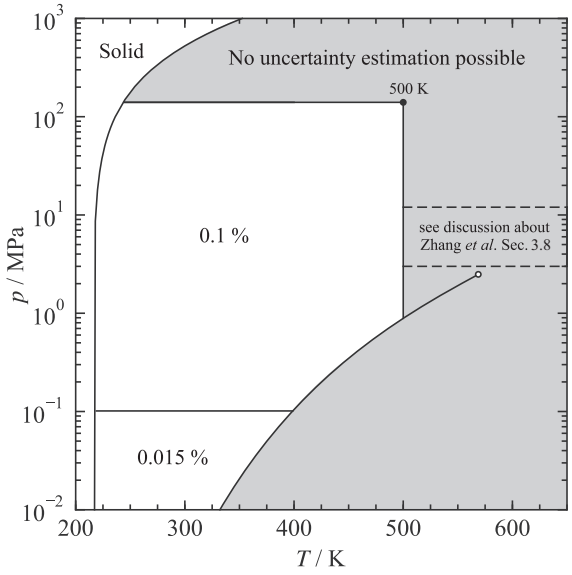

Figure 22. Estimated expanded relative uncertainties ($k = 2$) in speed of sound $\Delta w/w$ of the new EOS.

est temperature, since the data point is very close to the phase boundary. However, neither indications of this nor statements about the uncertainty in temperature measurement could be obtained from the Russian publication. In the vapor phase, the data of Hossenlopp and Scott[13] were used for adjusting the new EOS. It is important to consider that Hossenlopp and Scott[13] also performed measurements at pressures below ambient pressure and, therefore, all data points are located in the vapor phase. Consequently, the illustrated phase boundary in

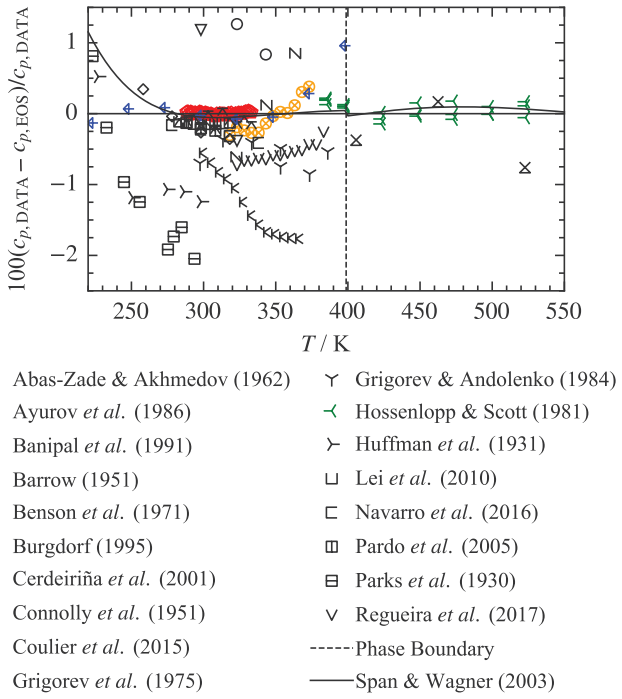

Figure 23. Percentage deviation of selected isobaric heat capacity data at atmospheric pressure from the new EOS and the EOS of Span and Wagner.[2]

Fig. 23 is not valid for this dataset, since it corresponds to the saturation temperature at ambient pressure. The experimental uncertainty of the results determined by vapor-flow calorimetry is reported to be 0.2 %. However, it is not clarified if it is a standard or expanded uncertainty. Nevertheless, except for one data point (0.22%), all data are reproduced within 0.2% with an AARD of 0.10 %.

Figure 24 shows the available isobaric heat capacity data at elevated pressures along with the discussed atmospheric datasets as reference points. At pressures up to 10 MPa, the new EOS agrees best with the results of Banipal *et al*.,[114] who measured data with a Calvet calorimeter and the differential incremental method. Uncertainties in heat capacity, temperature, and pressure are stated as 0.01 J K^{-1} g^{-1}, 0.05 K, and 0.01 MPa. Based on this information, we determined a combined uncertainty ($k = 2$) of 0.85 %. Except for a single data point at 10 MPa, the data of Banipal *et al*.[114] are reproduced within 0.7 %. In the pressure range above 10 MPa, only two datasets of Kuznetsov *et al*.[264] and Czarnota[265] are available. Kuznetsov *et al*.[264] do not provide any uncertainty analysis but estimate the uncertainty from 0.35 % to 0.5 %. However, since the data along lower isobars exhibit a high scatter, they deviate from the results of Banipal *et al*.,[114] and the Russian publication contains less information about the measurement method and its error analysis, we assume that the uncertainty estimation of Kuznetsov *et al*.[264] was too optimistic. The data of Czarnota,[265] on the other hand, show a systematic offset in the overlapping pressure range with Kuznetsov *et al*.[264] and deviate up to 11 % from the new EOS, although the experimental uncertainty of the isobaric heat capacities was esti-

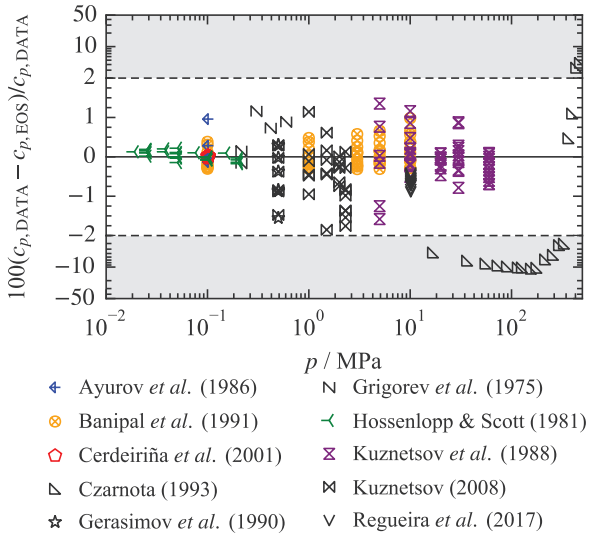

Figure 24. Percentage deviation of selected isobaric heat capacity data from the new EOS. The ordinate is linearly scaled between the dashed lines and logarithmically scaled in the gray filled regions.

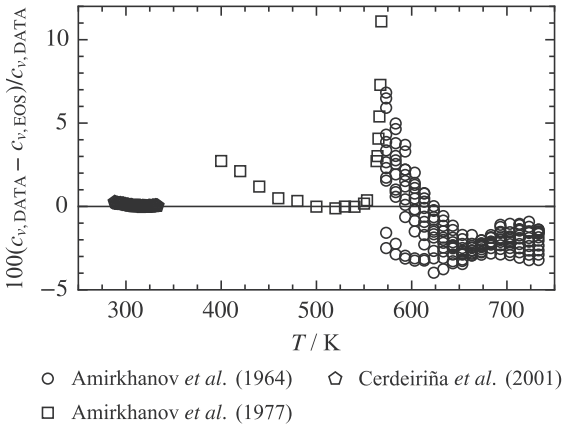

Figure 25. Percentage deviation of isochoric heat capacity data from the new EOS.

mated by the author to be 2 %. However, the core apparatus of the experimental setup was also used for calorimetric measurements on pentane, hexane, and heptane,[266] and even though the uncertainty of these results was estimated to be only 1 %, all data show significantly higher deviations from the reference EOS. The data are reproduced by the corresponding reference EOS with an AARD of 5.4 % for heptane, 5.8 % for hexane, and 3.4 % for pentane. Therefore, we assume that the data do not describe the isobaric heat capacity correctly and consequently the data of Czarnota[265] were not used for fitting the new EOS.

Based on the reproduction of the datasets of Cerdeiriña *et al.*,[91] Ayurov *et al.*,[263] and Hossenlopp and Scott,[13] the uncertainty of the new EOS at atmospheric pressure is estimated to be 0.1 % in the liquid and 0.2 % in the vapor phase. For pressures up to 60 MPa and temperatures up to 635 K, we estimate the uncertainty to be 1 %, even though it might be lower at pressures below 10 MPa.

The deviations of the available isochoric heat capacity datasets are shown in Fig. 25. Compared to the isobaric heat capacities, the database is even more limited in its quantity and quality. Aside from the data of Cerdeiriña *et al.*,[91] who calculated isochoric heat capacities from isobaric heat capacities, homogeneous densities, and speed of sound data at atmospheric pressure, only two datasets of Amirkhanov *et al.*[267,268] are available. For their calculations, Cerdeiriña *et al.*[91] specify an uncertainty of 0.2 J mol^{-1} K^{-1}, corresponding to an average relative uncertainty of 0.1 %. Since the new EOS was fitted to the experimentally determined properties of Cerdeiriña *et al.*[91] (see Sec. 3.4 and 3.8), the EOS consequently also agrees with the calculated isochoric heat capacities.

The datasets of Amirkhanov *et al.*[267,268] cover parts of the saturated liquid phase as well as the critical and supercritical regions. For both datasets, an increase in deviation is observed near the critical temperature, which is attributable to a critical point phenomena. Upon approaching the critical temperature, the isochoric heat capacity exhibits a sharp increase and becomes, in theory, infinitely large at the critical point. However, since this special behavior can only be modeled qualitatively with the functional form of the new EOS, even small differences in the steep slope lead to high deviations. Nevertheless, even within the supercritical range, the data show high deviations of up to 5 %, which could not be reduced significantly during the entire fitting process. Since we could not obtain any information about the uncertainty of the data from the Russian publication, we compared their results for *n*-heptane, which are also part of the publication, with the current reference model for *n*-heptane[269] to assess the quality of the data. The results were very similar to the results for *n*-octane and showed deviations of up to 10 %. These findings are also in agreement with the statements of Wagner and Pruß[19] and Herrig *et al.*,[5] who found high uncertainties and inconsistencies in isochoric heat capacity data for ordinary and heavy water measured from Amirkhanov *et al.*[270] at the Dagestan Scientific Center. Therefore, we decided to neglect these data in the fitting process, although comparisons were still viewed on a continues basis.

Due to the lack of reliable data, no uncertainty can be estimated for isochoric heat capacities calculated from the new EOS.

4. Physical Behavior

In addition to the most accurate possible representation of the available experimental database, the correct description of the fluid-specific physical behavior is of essential importance for the validity of an EOS. Therefore, the physical behavior of the developed EOS for *n*-octane is analyzed and evaluated in the following with the use of different characteristic thermodynamic properties. Since the EOS is also intended to be applied for the calculation of mixture properties, and mixture models are often evaluated in pressure and temperature regions outside of the range of validity of the pure-fluid EOS,

Table 15. AARD of isobaric and isochoric heat capacity data calculated with the new EOS and the EOS of Span and Wagner.[2]

Reference	N	(T_{min} - T_{max}) / K	(p_{min} - p_{max}) / MPa	$AARD_{SW}$	$AARD_{This\ work}$
		Isobaric heat capacity c_p			
Abas-Zade and Akhmedov (1962)[271]	2	323 - 344	0.101325	1.1	1
Akhmedov (1970)[272]	1	293.14	0.101325	0.95	0.91
Andreoli-Ball *et al*. (1988)[273]	1	298.14	0.101325	0.53	0.48
Ayurov *et al*. (1986)[263]	8	223 - 399	0.101325	0.34	0.21
Banipal *et al*. (1991)[114]	60	318 - 374	0.1 - 10.0	0.22	0.24
Barrow (1951)[15]	3	405 - 523	0.101325	0.42	0.43[a]
Benson *et al*. (1971)[117]	4	258 - 319	0.101325	0.18	0.25
Benson & D'Arcy (1986)[274]	1	298.14	0.101325	0.088	0.14
Burgdorf (1995)[122]	2	298 - 324	0.101325	0.78	0.78
Calvo *et al*. (1998)[123]	1	298.15	0.101325	0.2	0.25
Cerdeiriña *et al*. (2001)[91]	46	288 - 334	0.101325	0.05	0.013
Cerdeiriña *et al*. (2000)[275]	1	298.15	0.101325	0.002	0.051
Connolly *et al*. (1951)[276]	13	299 - 367	0.101325	1.3	1.3
Costas & Patterson (1985)[277]	1	298.19	0.101325	0.52	0.47
Coulier *et al*. (2015)[278]	11	283 - 334	0.101325	0.095	0.12
Czarnota (1993)[265]	18	298 - 300	0.1 - 474	6.2	6
Filippov & Laushkina (1984)[279]	1	293	0.101325	0.67	0.71
Gerasimov *et al*. (1990)[16]	7	476 - 633	0.5	0.65	0.61[b]
Grigorev *et al*. (1975)[280]	9	303 - 463	<0.1 - 0.6	0.52	0.54
Grigorev & Andolenko (1984)[281]	7	297 - 387	0.101325	0.57	0.58
Grolier *et al*. (1981)[282]	1	298.14	0.101325	0.1	0.15
Hossenlopp & Scott (1981)[13]	28	385 - 524	<0.1 - 0.2	0.13	0.10[c]
Huffman *et al*. (1931)[283]	5	227 - 299	0.101325	1	1
Kuznetsov *et al*. (1988)[264]	49	329 - 633	5.0 - 30.0	0.5	0.38[d]
Kuznetsov (2008)[284]	34	476 - 633	0.5 - 2.3	1.6	0.65[e]
Lainez *et al*. (1985)[285]	1	298.14	0.101325	0.24	0.29
Lainez *et al*. (1992)[286]	1	298.15	0.101325	0.31	0.35
Lainez *et al*. (1995)[287]	1	298.15	0.101325	0.25	0.3
Lainez *et al*. (1985)[288]	1	298.14	0.101325	0.06	0.11
Lei *et al*. (2010)[165]	8	283 - 319	0.101325	0.094	0.14
Nakai *et al*. (1991)[289]	1	298.15	0.101325	0.053	0.1
Navarro *et al*. (2016)[182]	4	278 - 339	0.101325	0.25	0.28
Pardo *et al*. (2005)[185]	3	288 - 309	0.101325	0.15	0.19
Parks *et al*. (1930)[290]	8	223 - 294	0.101325	1.4	1.3
Perez-Casas *et al*. (1988)[291]	1	298.14	0.101325	0.53	0.48
Regueira *et al*. (2017)[292]	29	323 - 399	0.1 - 10.1	0.63	0.59
Roux *et al*. (1984)[293]	1	298.14	0.101325	0.12	0.17
Soejima *et al*. (1991)[294]	1	298.15	0.101325	0.053	0.1
Tardajos *et al*. (1986)[235]	1	298.14	0.101325	0.53	0.48
Trejo *et al*. (1991)[295]	1	298.15	0.101325	0.53	0.48
		Isochoric heat capacity c_v			
Amirkhanov *et al*. (1964)[267]	204	573 - 734	2.2 - 68.2	2.3	2.1
Amirkhanov *et al*. (1977)[268]	14	399 - 569	0.1 - 2.5	5.9	2.4
Cerdeiriña *et al*. (2001)[91]	46	288 - 334	0.101325	2.7	0.072

[a] dataset lies in the homogeneous vapor region
[b] dataset contains data in the homogeneous vapor and supercritical region at low (LD) densities: $AARD_{vap} = 0.91$ %, $AARD_{LD} = 0.20$ %
[c] dataset lies in the homogeneous vapor region
[d] dataset contains data in the homogeneous liquid and supercritical region at medium (MD) and high (HD) densities: $AARD_{liq} = 0.27$ %, $AARD_{MD} = 1.5$ %, $AARD_{HD} = 0.5$ %
[e] dataset contains data in the homogeneous vapor, critical, and supercritical region at low (LD) densities: $AARD_{vap} = 0.71$ %, $AARD_{crit} = 1.4$ %, $AARD_{LD} = 0.48$ %

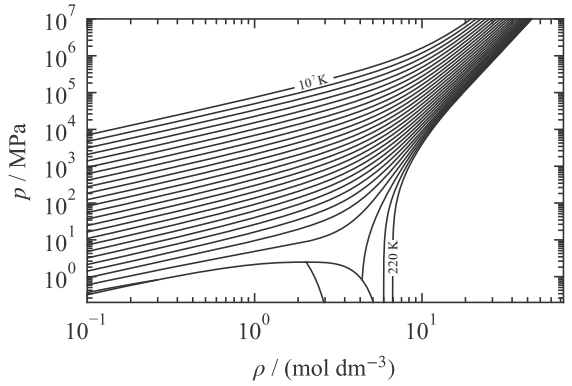

Figure 26. p,ρ-diagram along isotherms up to 10^7 K calculated with the new EOS.

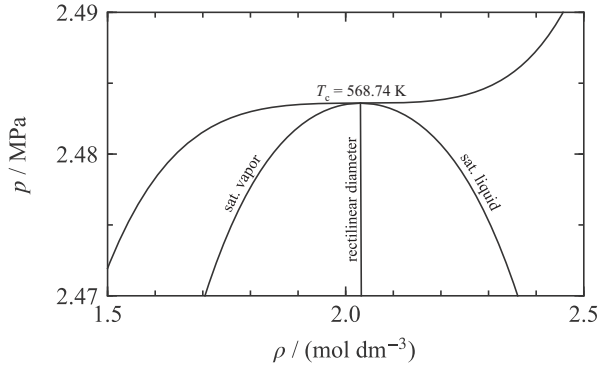

Figure 27. p,ρ-diagram showing the critical isotherm, phase boundary, and rectilinear diameter in the critical region calculated from the new EOS.

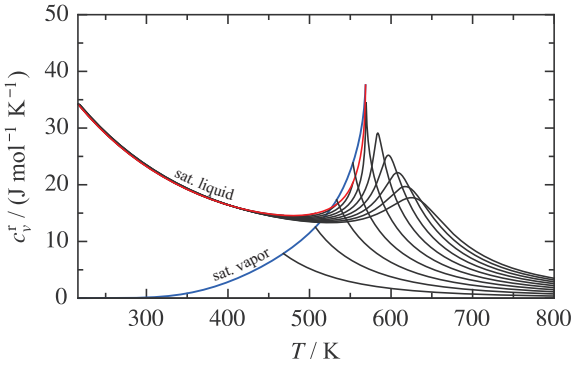

Figure 28. Residual isochoric heat capacity along isobars up to 5 MPa calculated with the new EOS.

Table 16. Definition of the Ideal curve (ID), Boyle curve (BL), Joule-Thomson inversion curve (JT), and Joule inversion curve (JI) in terms of the compressibility factor and their relations to the residual part of the reduced Helmholtz energy.

Definition		Relation to α and its derivatives
ID:	$Z = 1$	$\left(\frac{\partial \alpha^r}{\partial \delta}\right)_\tau = 0$
BL:	$\left(\frac{\partial Z}{\partial \rho}\right)_T = 0$	$\left(\frac{\partial \alpha^r}{\partial \delta}\right)_\tau + \delta\left(\frac{\partial^2 \alpha^r}{\partial \delta^2}\right)_\tau = 0$
JT:	$\left(\frac{\partial Z}{\partial T}\right)_p = 0$	$\left(\frac{\partial \alpha^r}{\partial \delta}\right)_\tau + \delta\left(\frac{\partial^2 \alpha^r}{\partial \delta^2}\right)_\tau + \tau\left(\frac{\partial^2 \alpha^r}{\partial \delta \partial \tau}\right) = 0$
JI:	$\left(\frac{\partial Z}{\partial T}\right)_\rho = 0$	$\left(\frac{\partial^2 \alpha^r}{\partial \delta \partial \tau}\right) = 0$

an important part of the physical analysis is the investigation of the extrapolation behavior.

Findings about the physical behavior of thermal properties calculated from the EOS can be gained from Fig. 26. In the double logarithmic scaled pressure-density diagram, the correct extrapolation behavior is indicated by converging isotherms at high pressures and densities, which should not intersect. Figure 26 shows that the new EOS fulfills this requirement even for isotherms of up to 10^7 K.

Another important criterion for assessing the physical behavior of an EOS results from the course of the critical isotherm in the critical region, which is illustrated in more detail in Fig. 27. The first and second derivatives of pressure with respect to density become zero at the critical point. Furthermore, the rectilinear diameter $\rho_{RD} = (\rho' + \rho'')/2$ should be nearly linear without any unreasonable deformations. Since the new EOS was constrained to these requirements, it exhibits the desired behavior and shows a saddle point along of the critical isotherm at the critical point.

More information about the critical region and the physical behavior in general can be obtained from the residual isochoric heat capacity, which is shown in Fig. 28. An important characteristic of this property is defined by the course of the saturation curves. They should intersect once and converge with positive slope and curvature approaching an infinite maximum at the critical point. Furthermore, the isobars should exhibit negative slope with positive curvature at low temperatures. At high temperatures, the residual isochoric heat capacity should approach zero to ensure the correct transition to the ideal gas. Even though no classical EOS can produce the theoretically correct divergence of c_v, the new EOS exhibits a distinct maximum at the critical temperature and satisfies the other requirements, as shown in Fig. 28.

A very sensitive and versatile test for evaluating the extrapolation behavior of an EOS is defined by the so called "ideal curves", along which the properties of the real fluid correspond to the properties of the hypothetical ideal gas at the same temperature and density. Even though they can be formulated for almost every thermodynamic property, the definition for the compressibility factor Z and its derivatives is commonly used, since their formulations include important derivatives of the residual Helmholtz energy, which are also required for the calculation of a multitude of other thermodynamic properties. Their definitions, including their relations to the Helmholtz energy, are given in Table 16.

In Fig. 29, the ideal curves calculated from the new EOS are compared to those calculated from the EOS of Span and Wagner[2] in a reduced pressure-temperature diagram with logarithmic axes. While the Joule inversion curve and the Joule-Thomson inversion curve calculated from the EOS of

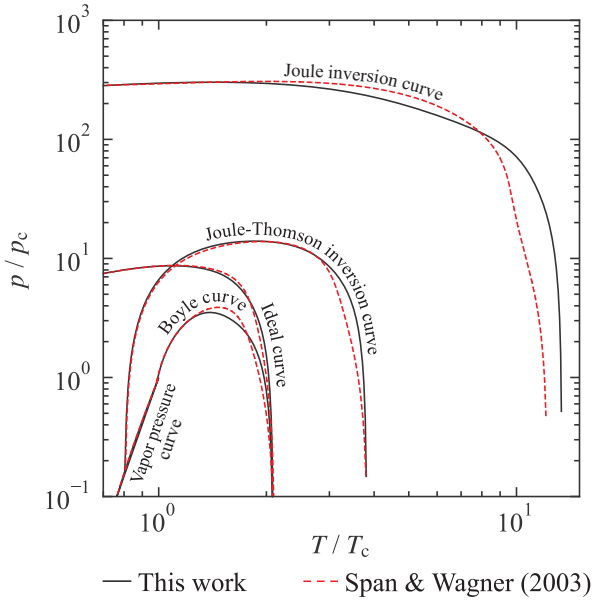

Figure 29. Ideal curves calculated from the new EOS and the EOS of Span and Wagner.[2]

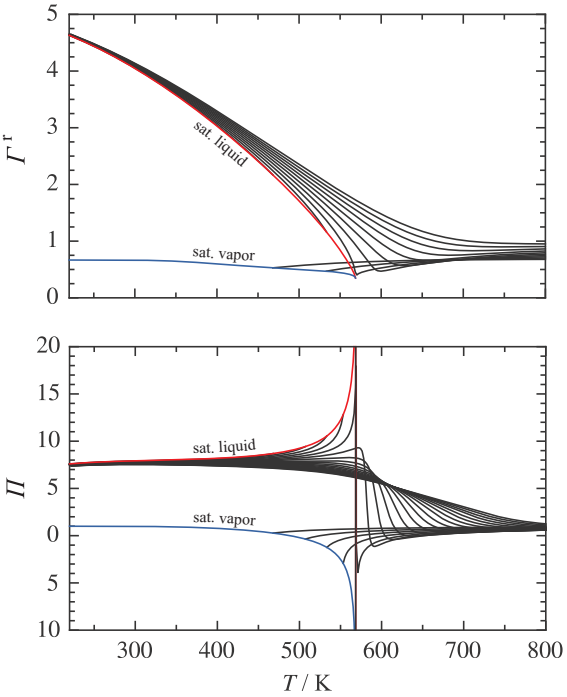

Figure 30. Residual Grüneisen parameter (top) and phase identification parameter (bottom) along isobars up to 10 MPa calculated with the new EOS.

Span and Wagner[2] exhibit slight deformations in the high-temperature region, the new EOS shows smooth behavior without any discontinuities over the entire temperature and pressure range along all curves, which indicates reasonable extrapolation behavior.

In addition to the discussed examples, a variety of other thermodynamic properties, like the pseudo Grüneisen parameter[296,297] or phase identification parameter,[298] were evaluated and monitored during the development process. The pseudo Grüneisen parameter Γ is valuable for assesing the extrapolation behavior of an EOS, as it is defined by the ratio of the first pressure derivative with respect to temperature at constant density and the isochoric heat capacity.

$$\Gamma^{\mathrm{r}} = \frac{(\partial p/\partial T)_\rho}{\rho/c_v^{\mathrm{r}}} \tag{20}$$

Thus, it combines thermal and caloric properties, which is of special interest for the validation of EOS. Initially, the parameter was introduced for the description of crystalline properties,[299] but meanwhile its use is also common for the evaluation of the extrapolation behavior of an EOS in the fluid state region.[296,297] However, since the pseudo Grüneisen parameter is intended for the validation of the residual part of the EOS, the contribution of the ideal gas part to the isochoric heat capacity is neglected. Due to the correlations of the pressure derivative and the isochoric heat capacity in terms of the Helmholtz energy, the course of the Grüneisen parameter versus temperature is very similar to the speed of sound (see Sec. 3.8). Consequently, the same evaluation criteria are applied. The phase identification parameter Π was introduced by Venkatarathnam and Oellrich[298] to determine the phase of a fluid at a given state point without the requirement of a complex iterative determination of the phase boundary. Due to the combination of different pressure derivatives (cf. Eq. 21), it provides valuable information about the quality of an EOS.

$$\Pi = 2 - \rho\left(\frac{(\partial^2 p/\partial\rho\partial T)}{(\partial p/\partial T)_\rho} - \frac{(\partial^2 p/\partial\rho^2)_T}{(\partial p/\partial\rho)_T}\right) \tag{21}$$

A characteristic of this property is the distinct maximum of the saturated liquid curve and the minimum of the saturated vapor curve at the critical point. Furthermore, the isolines should not exhibit any discontinuities or deformations. Both the residual Grüneisen parameter and the phase identification parameter are shown as a function of temperature with lines of constant pressure in Fig. 30. Based on the analysis of a multitude of different thermodynamic properties, we conclude that the new EOS exhibits correct physical and extrapolation behavior over wide temperature and pressure ranges.

5. Conclusion

A new fundamental EOS in terms of the Helmholtz energy was developed for *n*-octane. The ideal part of the EOS consists of a constant for the temperature-independent contribution of translation and rotation, and three Planck-Einstein terms for vibration. The residual part contains five polynomial, five exponential, and four Gaussian bell-shaped terms. For calculations of the vapor-liquid equilibrium, three auxiliary equations for vapor pressure, saturated vapor density, and saturated liquid density were developed.

Based on the available experimental data, the presented EOS is valid in a temperature range from the triple-point temperature T_{tp} = 216.37 K to T_{max} = 650 K with a maximum

pressure of p_{max} = 1000 MPa. The uncertainty in the calculation of homogeneous densities in the liquid phase at ambient pressure is 0.03 % and 0.5 % for pressures up to 200 MPa at temperatures below 270 K. In the temperature range between 270 K and 440 K, the uncertainty is estimated to be 0.1 %. Outside this range, the uncertainty in the liquid phase up to 600 K and 100 MPa increases up to 0.5 %. Vapor densities can be determined with an accuracy of 0.5 % for temperatures below 600 K. At higher temperatures and pressures, including the supercritical region, an uncertainty of up to 3 % is estimated. Saturated liquid densities can be determined with an uncertainty of 0.3 %. The accuracy of the new EOS in vapor pressures is estimated to be 0.03 % for temperatures above 400 K up to the critical point. Between 320 K and 400 K, the uncertainty is estimated to be 0.02 %. Due to the inconsistent data situation below 320 K, no uncertainty can be estimated for this region. The heat of vaporization is represented with an uncertainty of 0.1 % for temperatures up to 425 K and 2 % above 425 K. The uncertainty in speed of sound in the homogeneous liquid phase at atmospheric pressure is 0.015 %. For the pressure range up to 140 MPa and temperatures up to 500 K, the uncertainty is estimated to 0.1 %. Outside this region, no uncertainties can be estimated. Isobaric heat capacity in the liquid phase can be calculated with an uncertainty of 0.1 % and in the vapor phase with 0.2 % at atmospheric pressure. For pressures up to 60 MPa and temperatures up to 635 K, the estimated uncertainty is 1 %.

Compared to the EOS of Span and Wagner,[2] the greatest improvements were achieved in the description of speed of sound over the entire fluid region and densities in the extended critical region. By simultaneously optimizing the ideal-gas and residual contributions, the uncertainty in speed of sound in the homogeneous liquid region could be reduced to one-twentieth of the uncertainty of the EOS of Span and Wagner.[2] Another significant improvement was achieved by changing the critical properties to slightly lower values from the literature (see Table 1). This change was not only helpful in representing density data in the extended critical region more accurately, but it also had a positive effect on the description of other thermodynamic properties. Furthermore, the critical properties represent a fixed end point of the saturation curve. Consequently, properties along the saturation curve and near the critical region can only be described accurately if the critical point is correctly defined. Compared to the EOS of Span and Wagner,[2] the estimated uncertainty in densities in the extended critical region and vapor pressures could be reduced to one-fifth and one-tenth, respectively. In addition to decreasing the uncertainty of specific properties, the range of validity of the EOS could be increased by 50 K and 900 MPa based on the comprehensive database. However, due to an insufficient or low-quality data situation, the new EOS holds potential for improvement in the description of vapor densities, saturated speeds of sound, and third virial coefficients. For a more accurate description of these properties, new highly accurate measurements would be of great benefit.

The new EOS is already implemented in the thermodynamic software tools REFPROP,[300] TREND,[301] and CoolProp.[302] Test values calculated with TREND[301] for computer implementation are given in Table 17. The number of digits of the properties is not related to the uncertainty of the model.

6. Supplementary Material

The supplementary material comprises a fluid file with the parameters of the equation for application in REFPROP,[300] TREND,[301] and CoolProp.[302] Deviation plots of the available density and speed of sound data divided into isotherms, and a deviation plot of all available vapor-pressure data are also included.

7. Author Declarations

7.1. Conflict of interest

The authors have no conflicts to disclose.

8. Data Availability

Data sharing is not applicable to this article as no new data were created in this study.

References

[1] National Center for Biotechnology Information, *PubChem Compound Summary for CID 356. https://pubchem.ncbi.nlm.nih.gov/compound/Octane. Accessed 24 March 2021* (2021), URL `https://pubchem.ncbi.nlm.nih.gov/compound/Octane`.
[2] R. Span and W. Wagner, Int. J. Thermophys. **24**, 1 (2003).
[3] E. W. Lemmon and R. T. Jacobsen, J. Phys. Chem. Ref. Data **34**, 69 (2005).
[4] E. W. Lemmon, M. O. McLinden, and W. Wagner, J. Chem. Eng. Data **54**, 3141 (2009).
[5] S. Herrig, M. Thol, A. H. Harvey, and E. W. Lemmon, J. Phys. Chem. Ref. Data **47**, 043102 (2018).
[6] M. Thol, M. Richter, E. F. May, E. W. Lemmon, and R. Span, J. Phys. Chem. Ref. Data **48**, 033102 (2019).
[7] R. Span, *Multiparameter equations of state: An accurate source of thermodynamic property data* (Springer-Verlag, Berlin and Heidelberg, 2000).
[8] O. Kunz, R. Klimeck, W. Wagner, and M. Jaeschke, *The GERG-2004 wide-range equation of state for natural gases and other mixtures*, vol. 15 of *GERG technical monograph* (VDI-Verl., Düsseldorf, 2007).
[9] A. Kreglewski and W. B. Kay, J. Phys. Chem. **73**, 3359 (1969).
[10] J. B. Ott and R. J. Goates, J. Chem. Thermodyn. **15**, 267 (1983).
[11] M. E. Wieser, N. Holden, T. B. Coplen, J. K. Böhlke, M. Berglund, W. A. Brand, P. de Bièvre, M. Gröning, R. D. Loss, J. Meija, et al., Pure Appl. Chem. **85**, 1047 (2013).
[12] E. Tiesinga, P. J. Mohr, D. B. Newell, and B. N. Taylor, Rev. Mod. Phys. **93**, 025010 (2021).
[13] I. A. Hossenlopp and D. W. Scott, J. Chem. Thermodyn. **13**, 415 (1981).
[14] K. S. Pitzer, Ind. Eng. Chem. **36**, 829 (1944).
[15] G. M. Barrow, J. Am. Chem. Soc. **73**, 1824 (1951).
[16] A. A. Gerasimov, M. A. Kuznetsov, V. E. Kharin, and B. A. Grigorev, Viniti, Code 4645-B90 pp. 1–14 (1990).
[17] V. Štejfa, M. Fulem, and K. Růžička, J. Chem. Phys. **150**, 224101 (2019).
[18] M. B. Ewing and J. C. Sanchez Ochoa, Fluid Phase Equilib. **210**, 277 (2003).
[19] W. Wagner and A. Pruß, J. Phys. Chem. Ref. Data **31**, 387 (2002).

Table 17. Test values in the single-phase region for computer implementation.

T / K	ρ / mol m^{-3}	p / MPa	c_p / J mol^{-1} K^{-1}	w / m s^{-1}	h / J mol^{-1}	s / J mol^{-1} K^{-1}	a / J mol^{-1}
500	200	0.679567285	308.0591118	158.7971365	59003.95193	127.0152476	−7901.508319
500	5000	22.12393515	337.6029454	741.4733129	33933.78761	66.14973635	−3565.867594
700	2000	7.191953009	434.3588772	184.5490128	114104.516	206.0345238	−33715.62722

[20]C. B. Willingham, W. J. Taylor, J. M. Pignocco, and F. D. Rossini, J. Res. Natl. Bur. Stan. **35**, 219 (1945).
[21]G. F. Carruth and R. Kobayashi, J. Chem. Eng. Data **18**, 115 (1973).
[22]A. Ait-Kaci, J. Jose, and G. Belaribi, Int. Data Series Sel. Data Mixtures Ser. A **2**, 105 (1989).
[23]W. Arlt, Ph.D. Thesis, Universität Dortmund, Dortmund (1981).
[24]A. G. Badalyan, A. S. Keramidi, D. S. Kurumov, and B. A. Grigorev, Izv. Vyssh. Uchebn. Zaved. Neft Gaz pp. 54–57 (1986).
[25]I. Batiu, Eldata Int. Electron. J. Phys.-Chem. Data **5**, 1 (1999).
[26]H. Ben-makhlouf Hakem, A. Ait-Kaci, and J. Jose, Fluid Phase Equilib. **232**, 189 (2005).
[27]G. Boukais-Belaribi, B. F. Belaribi, A. Ait-Kaci, and J. Jose, Fluid Phase Equilib. **167**, 83 (2000).
[28]J. F. Connolly, Proc. - Am. Pet. Inst., Sect. 3 **45**, 62 (1965).
[29]J. F. Connolly and G. A. Kandalic, J. Chem. Eng. Data **7**, 137 (1962).
[30]J. T. Cripwell, C. E. Schwarz, and A. J. Burger, J. Chem. Eng. Data **61**, 2353 (2016).
[31]A. Dejoz, V. González-Alfaro, P. J. Miguel, and M. I. Vázquez, J. Chem. Eng. Data **41**, 93 (1996).
[32]A. del Rio, B. Coto, C. Pando, and J. A. R. Renuncio, Fluid Phase Equilib. **200**, 41 (2002).
[33]W. A. Felsing and G. M. Watson, J. Am. Chem. Soc. **64**, 1822 (1942).
[34]L. Fernández, E. Pérez, J. Ortega, J. M. Canosa, and J. Wisniak, J. Chem. Eng. Data **55**, 5519 (2010).
[35]M. Gracia, F. Sánchez, P. Pérez, J. Valero, and C. G. Losa, J. Chem. Thermodyn. **24**, 843 (1992).
[36]J. Gregorowicz, K. Kiciak, and S. Malanowski, Fluid Phase Equilib. **38**, 97 (1987).
[37]A. Grenner, M. Klauck, and J. Schmelzer, Fluid Phase Equilib. **233**, 170 (2005).
[38]H. Hakem and A. Ait-Kaci, Int. Data Series Sel. Data Mixtures Ser. A **30**, 277 (2002).
[39]D. V. S. Jain and O. P. Yadav, Indian J. Chem. **9**, 432 (1971).
[40]C. R. Koppany and C. J. Rebert, *Vapor-Liquid for the Benzene-n-Octane System Near the Region of the Critical Locus* (American Institute of Chemical Engineers, New York, 1973).
[41]E. H. Leslie and A. R. Carr, Ind. Eng. Chem. **17**, 810 (1925).
[42]G. Li and Z. Li, J. Chem. Eng. Data **58**, 2044 (2013).
[43]E. K. Liu and R. R. Davison, J. Chem. Eng. Data **26**, 85 (1981).
[44]J. H. McMicking and W. B. Kay, Proc. - Am. Pet. Inst., Sect. 3 **44**, 75 (1965).
[45]M. A. Michou-Saucet, J. Jose, C. Michou-Saucet, and J. C. Merlin, Thermochim. Acta **75**, 85 (1984).
[46]J. Millat, E. Bich, H. Hendl, and A. K. Neumann, High Temp. - High Press. **26**, 251 (1994).
[47]K. Moodley and J. D. Raal, J. Chem. Eng. Data **65**, 3297 (2020).
[48]C. F. Muendel, Z. Phys. Chem. **85**, 435 (1913).
[49]J. Ortega and F. Espiau, Ind. Eng. Chem. Res. **42**, 4978 (2003).
[50]E. Otsa, I. Kirjanen, and L. S. Kudryavtseva, Eesti NSV Tead. Akad. Toim. Keem. **28**, 113 (1979).
[51]R. E. Perry and G. Thodos, Ind. Eng. Chem. **44**, 1649 (1952).
[52]Z. Plesnar, Y. H. Fu, S. I. Sandler, and H. Orbey, J. Chem. Eng. Data **41**, 799 (1996).
[53]P. Reddy, J. D. Raal, and D. Ramjugernath, Fluid Phase Equilib. **358**, 121 (2013).
[54]M. S. Rozhnov, Khim. Prom. **43**, 288 (1967).
[55]N. V. Shevchenko and P. M. Kharchenko, Izv. Vyssh. Uchebn. Zaved. Neft Gaz pp. 62–64 (1987).
[56]J. S. Stadnicki, Rocz. Chem. **37**, 1211 (1963).
[57]C. Wang, H. Li, L. Ma, and S. Han, J. Chem. Eng. Data **48**, 1120 (2003).
[58]J. Wisniak, G. Galindo, R. Reich, and H. Segura, Phys. Chem. Liq. **37**, 649 (1999).
[59]B. Woringer, Z. Phys. Chem. **34**, 257 (1900).
[60]H. S. Wu, W. E. Locke, and S. I. Sandler, J. Chem. Eng. Data **36**, 127 (1991).
[61]A. Yahiaoui, J. A. González, A. Ait-Kaci, J. Jose, and H. V. Kehiaian, Fluid Phase Equilib. **98**, 179 (1994).
[62]C. P. Yang and M. van Winkle, Ind. Eng. Chem. **47**, 293 (1955).
[63]S. Young, Proc. R. Irish Acad. **38**, 65 (1928).
[64]S. Young, Sci. Proc. Roy. Dublin Soc. **12**, 374 (1910).
[65]S. Young, The London, Edinburgh and Dublin Philosophical Magazine **50**, 291 (1900).
[66]V. Majer, V. Svoboda, S. Hála, and J. Pick, Collect. Czech. Chem. Commun. **44**, 637 (1979).
[67]N. S. Osborne and D. C. Ginnings, J. Res. Natl. Bur. Stan. **39**, 453 (1947).
[68]E. Morawetz, I. Elvebredd, J. Brunvoll, G. Hagen, and J. Paasivirta, Acta Chem. Scand. **22**, 1509 (1968).
[69]I. Wadsö, Acta Chem. Scand. **14**, 566 (1960).
[70]A. Bashir-Hashemi, J. S. Chickos, W. Hanshaw, H. Zhao, B. S. Farivar, and J. F. Liebman, Thermochim. Acta **424**, 91 (2004).
[71]I. A. Dibrov, Y. N. Nikolaeva, and V. L. Ugolkov, Zh. Prikl. Khim. **72**, 384 (1999).
[72]D. V. Fenby, J. R. Khurma, Z. S. Kooner, T. E. Block, C. M. Knobler, J. Reeder, and R. L. Scott, Aust. J. Chem. **33**, 1927 (1980).
[73]R. Fuchs, J. H. Hallman, and M. O. Perlman, Can. J. Chem. **60**, 1832 (1982).
[74]D. J. Graue, V. M. Berry, and B. H. Sage, Hydrocarbon Process. **45**, 191 (1966).
[75]J. H. Hallman, W. K. Stephenson, and R. Fuchs, Can. J. Chem. **61**, 2044 (1983).
[76]L. S. Kudryavtseva, M. Kuus, and N. Harsing, Eesti NSV Tead. Akad. Toim. Keem. **36**, 186 (1987).
[77]D. V. Matyushov and R. Schmid, Ber. Bunsen-Ges. Phys. Chem. **98**, 1590 (1994).
[78]R. A. McKay and B. H. Sage, J. Chem. Eng. Data **5**, 21 (1960).
[79]E. Morawetz, Chem. Scr. **1**, 103 (1971).
[80]E. Morawetz, S. Sunner, and Ö. Wiberg, Acta Chem. Scand. **17**, 473 (1963).
[81]P. Ulbig, M. Klüppel, and S. Schulz, Thermochim. Acta **271**, 9 (1996).
[82]R. M. Varushchenko, G. L. Galchenko, and V. A. Medvedev, Zh. Fiz. Khim. **51**, 992 (1977).
[83]I. Wadsö, Acta Chem. Scand. **20**, 536 (1966).
[84]H. Zhao, P. Unhannanant, W. Hanshaw, and J. S. Chickos, J. Chem. Eng. Data **53**, 1545 (2008).
[85]O. Prokopova, A. Blahut, M. Censky, M. Souckova, and V. Vins (24.06.2021), Twenty-First Symposium on Thermophysical Properties.
[86]T. J. Fortin, A. Laesecke, M. Freund, and S. Outcalt, J. Chem. Thermodyn. **57**, 276 (2013).
[87]D. González-Salgado, J. Troncoso, and L. Romani, in *Volume properties: Liquids, solutions and vapours*, edited by E. Wilhelm and T. M. Letcher (Royal Society of Chemistry, Cambridge, 2015), pp. 100–114.
[88]A. G. Badalyan, A. S. Keramidi, and D. S. Kurumov, Viniti, Code 3008-89 pp. 1–25 (1989).
[89]I. M. Abdulagatov, A. R. Bazaev, R. K. Gasanov, and A. E. Ramazanova, J. Chem. Thermodyn. **28**, 1037 (1996).
[90]I. M. Abdulagatov, A. R. Bazaev, E. A. Bazaev, S. P. Khokhlachev, M. B. Saidakhmedova, and A. E. Ramazanova, J. Solution Chem. **27**, 731 (1998).
[91]C. A. Cerdeiriña, C. A. Tovar, D. González-Salgado, E. Carballo, and L. Romaní, Phys. Chem. Chem. Phys. **3**, 5230 (2001).

[92]D. C. Landaverde-Cortes, A. Estrada-Baltazar, G. A. Iglesias-Silva, and K. R. Hall, J. Chem. Eng. Data **52**, 1226 (2007).
[93]F. Reyes-García and G. A. Iglesias-Silva, J. Chem. Eng. Data **62**, 2726 (2017).
[94]C. C. Chappelow, P. S. Snyder, and J. Winnick, J. Chem. Eng. Data **16**, 440 (1971).
[95]A. A. Abdussalam, G. R. Ivaniš, I. R. Radović, and M. L. Kijevčanin, J. Chem. Thermodyn. **100**, 89 (2016).
[96]Y. A. Sanmamed, A. Dopazo-Paz, D. González-Salgado, J. Troncoso, and L. Romaní, J. Chem. Thermodyn. **41**, 1060 (2009).
[97]D. R. Caudwell, J. P. M. Trusler, V. Vesovic, and W. A. Wakeham, J. Chem. Eng. Data **54**, 359 (2009).
[98]A. Schedemann, Ph.D. Thesis, Universität Oldenburg, Oldenburg (2013).
[99]L. Lugo, M. J. P. Comuñas, E. R. López, and J. Fernández, Fluid Phase Equilib. **186**, 235 (2001).
[100]G. Schilling, R. Kleinrahm, and W. Wagner, J. Chem. Thermodyn. **40**, 1095 (2008).
[101]B. Lagourette, C. Boned, H. Saint-Guirons, P. Xans, and H. Zhou, Meas. Sci. Technol. **3**, 699 (1992).
[102]G. S. Kell and E. Whalley, J. Chem. Phys. **62**, 3496 (1975).
[103]I. M. Abdulagatov and N. D. Azizov, J. Chem. Thermodyn. **38**, 1402 (2006).
[104]K. Liu, Y. Wu, M. A. McHugh, H. Baled, R. M. Enick, and B. D. Morreale, J. Supercrit. Fluids **55**, 701 (2010).
[105]M. Gomez-Nieto and G. Thodos, Ind. Eng. Chem. **16**, 254 (1977).
[106]A. Würflinger, Ber. Bunsen-Ges. Phys. Chem. **79**, 1195 (1975).
[107]A. Gayol, M. Iglesias, J. M. Goenaga, R. G. Concha, and J. M. Resa, J. Mol. Liq. **135**, 105 (2007).
[108]E. Aicart, G. Tardajos, and M. Díaz Peña, J. Chem. Eng. Data **25**, 140 (1980).
[109]V. Alonso, J. A. González, I. La García de Fuente, and J. C. Cobos, Thermochim. Acta **543**, 246 (2012).
[110]T. M. Aminabhavi and B. Gopalakrishna, J. Chem. Eng. Data **40**, 632 (1995).
[111]T. M. Aminabhavi, M. I. Aralaguppi, S. B. Harogoppad, and R. H. Balundgi, Fluid Phase Equilib. **72**, 211 (1992).
[112]T. M. Aminabhavi, M. I. Aralaguppi, G. Bindu, and R. S. Khinnavar, J. Chem. Eng. Data **39**, 522 (1994).
[113]A. F. A. Asfour, M. H. Siddique, and T. D. Vavanellos, J. Chem. Eng. Data **35**, 192 (1990).
[114]T. S. Banipal, S. K. Garg, and J. C. Ahluwalia, J. Chem. Thermodyn. **23**, 923 (1991).
[115]V. N. Belonenko, V. M. Troitsky, Y. E. Belyaev, J. H. Dymond, and N. F. Glen, J. Chem. Thermodyn. **32**, 1203 (2000).
[116]V. G. Ben'kovskii, M. K. Nauruzov, T. M. Bogoslovskaya, and Z. Serikov, Tr. Inst. Khim. Neft. Prir. Solei Akad. Nauk Kaz. SSR pp. 16–19 (1970).
[117]M. S. Benson and J. Winnick, J. Chem. Eng. Data **16**, 154 (1971).
[118]J. W. M. Boelhouwer, Physica **26**, 1021 (1960).
[119]D. W. Brazier and G. R. Freeman, Can. J. Chem. **47**, 893 (1969).
[120]P. W. Bridgman, Proc. Am. Acad. Arts Sci. **77**, 129 (1949).
[121]P. W. Bridgman, Proc. Am. Acad. Arts Sci. **66**, 185 (1931).
[122]R. Burgdorf, *Untersuchungen thermophysikalischer Eigenschaften ausgewählter organischer Flüssigkeitsgemische*, Berichte aus der Verfahrenstechnik (Shaker, Aachen, 1995), als ms. gedr ed.
[123]E. Calvo, P. Brocos, R. Bravo, M. Pintos, A. Amigo, A. H. Roux, and G. Roux-Desgranges, J. Chem. Eng. Data **43**, 105 (1998).
[124]Z. Chen, S. Liu, M. Huang, T. Yin, H. Wang, and W. Shen, J. Solution Chem. **42**, 1816 (2013).
[125]E. Cisneros-Pérez, C. M. Reza-San Germán, M. E. Manríquez-Ramírez, and A. Zúñiga-Moreno, J. Solution Chem. **41**, 1054 (2012).
[126]B. E. de Cominges, M. M. Piñeiro, E. Mosteiro, E. Mascato, M. M. Mato, T. P. Iglesias, and J. L. Legido, J. Therm. Anal. Calorim. **70**, 217 (2002).
[127]A. D'Aprano, I. D. Donato, and V. T. Liveri, J. Solution Chem. **19**, 711 (1990).
[128]R. Devi, S. Gahlyan, M. Rani, and S. Maken, J. Mol. Liq. **275**, 364 (2018).
[129]M. Díaz Peña and G. Tardajos, J. Chem. Thermodyn. **10**, 19 (1978).
[130]M. Dix, J. M. N. A. Fareleira, Y. Takaishi, and W. A. Wakeham, Int. J. Thermophys. **12**, 357 (1991).
[131]A. K. Doolittle and R. H. Peterson, J. Am. Chem. Soc. **73**, 2145 (1951).
[132]R. W. Dornte and C. P. Smyth, J. Am. Chem. Soc. **52**, 3546 (1930).
[133]V. Dumitrescu, M. M. Budeanu, S. Radu, and A. D. Cameniţă, Phys. Chem. Liq. **53**, 242 (2015).
[134]J. H. Dymond, J. Robertson, and J. D. Isdale, J. Chem. Thermodyn. **14**, 51 (1982).
[135]J. H. Dymond, J. Robertson, and J. D. Isdale, Int. J. Thermophys. **2**, 133 (1981).
[136]H. E. Eduljee, D. M. Newitt, and K. E. Weale, J. Chem. Soc. pp. 3086–3091 (1951).
[137]A. Estrada-Baltazar, G. A. Iglesias-Silva, and C. Caballero-Cerón, J. Chem. Eng. Data **58**, 3351 (2013).
[138]N. C. Exarchos, M. Tasioula-Margari, and I. N. Demetropoulos, J. Chem. Eng. Data **40**, 567 (1995).
[139]S. Fang, X. B. Zuo, X. J. Xu, and D. H. Ren, J. Chem. Thermodyn. **68**, 281 (2014).
[140]L. Fernández, J. Ortega, E. Pérez, F. Toledo, and J. M. Canosa, J. Chem. Eng. Data **58**, 686 (2013).
[141]E. B. Freyer, J. C. Hubbard, and D. H. Andrews, J. Am. Chem. Soc. **51**, 759 (1929).
[142]K. Fukuchi, K. Ogiwara, Y. Tashima, and S. Yonezawa, Ube Kogyo Koto Senmon Gakko Kenkyu Hokoku **29**, 93 (1983).
[143]J. Garbajosa, G. Tardajos, E. Aicart, and M. Díaz Peña, J. Chem. Thermodyn. **14**, 671 (1982).
[144]R. Garcia-Morales, O. Elizalde-Solis, A. Zúñiga-Moreno, C. Bouchot, F. I. Gómez-Ramos, and M. G. Arenas-Quevedo, Fuel **209**, 299 (2017).
[145]M. Garcia, C. Rey, V. P. Villar, and J. R. Rodriguez, J. Chem. Eng. Data **31**, 481 (1986).
[146]B. García, R. Alcalde, S. Aparicio, and J. M. Leal, Ind. Eng. Chem. Res. **41**, 4399 (2002).
[147]A. Gayol, L. M. Casás, R. E. Martini, A. E. Andreatta, and J. L. Legido, J. Chem. Thermodyn. **58**, 245 (2013).
[148]A. Z. Golik and I. I. Adamenko, Ukr. Fiz. Zh. **10**, 443 (1965).
[149]A. Z. Golik, I. I. Adamenko, and V. V. Borovik, Ukr. Fiz. Zh. **17**, 2075 (1972).
[150]X. Gong, Y. Guo, J. Xiao, Y. Yang, and W. Fang, J. Chem. Eng. Data **57**, 3278 (2012).
[151]C. González, M. Iglesias, J. Lanz, and J. M. Resa, Thermochim. Acta **328**, 277 (1999).
[152]A. R. H. Goodwin, E. P. Donzier, O. Vancauwenberghe, A. D. Fitt, K. A. Ronaldson, W. A. Wakeham, M. Manrique de Lara, F. Marty, and B. Mercier, J. Chem. Eng. Data **51**, 190 (2006).
[153]A. R. H. Goodwin, C. H. Bradsell, and L. S. Toczylkin, J. Chem. Thermodyn. **28**, 637 (1996).
[154]P. Gouel, Bull. Cent. Rech. Explor.-Prod. Elf-Aquitaine **2**, 211 (1978).
[155]K. R. Harris, R. Malhotra, and L. A. Woolf, J. Chem. Eng. Data **42**, 1254 (1997).
[156]W. Hayduk and C. F. Wong, Can. J. Chem. Eng. **68**, 653 (1990).
[157]M. Hussain and K. Moodley, J. Chem. Eng. Data **65**, 1636 (2020).
[158]N. Islam, B. Jamil, and S. A. A. Zaidi, Indian J. Chem. **11**, 266 (1973).
[159]N. Islam and B. Waris, Indian J. Chem. Sect. A **14**, 30 (1976).
[160]E. Jiménez, L. Segade, C. Franjo, H. Casas, J. L. Legido, and M. I. Paz Andrade, Fluid Phase Equilib. **149**, 339 (1998).
[161]E. Kiran and Y. L. Sen, Int. J. Thermophys. **13**, 411 (1992).
[162]A. Kumagai, D. Tomida, and C. Yokoyama, Int. J. Thermophys. **27**, 376 (2006).
[163]I. M. S. Lampreia and C. A. Nieto de Castro, J. Chem. Thermodyn. **43**, 537 (2011).
[164]H. Landolt and H. Jahn, Z. Phys. Chem. **10**, 289 (1892).
[165]Y. Lei, Z. Chen, X. An, M. Huang, and W. Shen, J. Chem. Eng. Data **55**, 4154 (2010).
[166]J. M. Lenoir, D. R. Robinson, and H. G. Hipkin, Proc. - Am. Pet. Inst., Div. Refin. **48**, 346 (1968).
[167]T. Ling and M. van Winkle, Ind. Eng. Chem. Chem. Eng. Data Series **3**, 88 (1958).
[168]Y. Liu, Y. Zhang, M. He, and N. Xin, J. Chem. Eng. Data **59**, 3852 (2014).
[169]J. S. López-Lázaro, G. A. Iglesias-Silva, A. Estrada-Baltazar, and J. Barajas-Fernández, J. Chem. Eng. Data **60**, 1823 (2015).
[170]P. Ma, Q. Zhou, Yang C., and S. Xia, Huagong Xuebao **55**, 1608 (2004).
[171]R. Manzoni-Ansidei, Boll. Sci. Fac. Chim. Ind. Bologna pp. 201–207 (1940).

[172]E. Mascato, L. Mussari, M. Postigo, A. B. Mariano, M. M. Piñeiro, J. L. Legido, and M. I. Paz Andrade, J. Chem. Eng. Data **54**, 453 (2009).
[173]J. S. Matos, J. L. Trenzado, E. González, and R. Alcalde, Fluid Phase Equilib. **186**, 207 (2001).
[174]K. Moodley, S. Adam, P. Naidoo, S. Naidu, and D. Ramjugernath, J. Chem. Eng. Data **63**, 4136 (2018).
[175]J. W. Moore and R. M. Wellek, J. Chem. Eng. Data **19**, 136 (1974).
[176]L. Morávková, Z. Wagner, and J. Linek, J. Chem. Thermodyn. **40**, 607 (2008).
[177]L. Morávková, Z. Wagner, K. Aim, and J. Linek, J. Chem. Thermodyn. **38**, 861 (2006).
[178]L. Morávková and J. Linek, J. Chem. Thermodyn. **40**, 671 (2008).
[179]L. Morávková and J. Linek, J. Chem. Thermodyn. **35**, 1119 (2003).
[180]L. Morávková and J. Linek, J. Chem. Thermodyn. **35**, 113 (2003).
[181]L. Mosteiro, A. B. Mariano, L. M. Casás, M. M. Piñeiro, and J. L. Legido, J. Chem. Eng. Data **54**, 1056 (2009).
[182]A. M. Navarro, B. García, F. J. Hoyuelos, I. A. Peñacoba, and J. M. Leal, Fluid Phase Equilib. **429**, 127 (2016).
[183]H. Ohji, H. Ogawa, S. Murakami, K. Tamura, and J. P. E. Grolier, Fluid Phase Equilib. **156**, 101 (1999).
[184]B. Orge, A. Rodriguez, J. M. Canosa, G. Marino, M. Iglesias, and J. Tojo, J. Chem. Eng. Data **44**, 1041 (1999).
[185]J. M. Pardo, C. A. Tovar, J. Troncoso, E. Carballo, and L. Romaní, Thermochim. Acta **433**, 128 (2005).
[186]E. Pérez, J. Ortega, L. Fernández, J. Wisniak, and J. Canosa, Fluid Phase Equilib. **412**, 79 (2016).
[187]A. Pimentel-Rodas, L. A. Galicia-Luna, and J. J. Castro-Arellano, J. Chem. Eng. Data **62**, 3946 (2017).
[188]M. Pirdashti, K. Movagharnejad, P. Akbarpour, E. N. Dragoi, and I. Khoiroh, Int. J. Thermophys. **41**, 35 (2020).
[189]P. P. Pugachevich and A. I. Cherkasskaya, Viniti, Code 1568-76 pp. 1–14 (1976).
[190]O. R. Quayle, R. A. Day, and G. M. Brown, J. Am. Chem. Soc. **66**, 938 (1944).
[191]M. Rama Rao, Indian J. Phys. Proc. Indian Ass. Cult. Sci. **14**, 109 (1940).
[192]M. Ramos-Estrada, G. A. Iglesias-Silva, K. R. Hall, and F. Castillo-Borja, J. Chem. Eng. Data **56**, 4461 (2011).
[193]A. Randová and L. Bartovská, J. Mol. Liq. **242**, 767 (2017).
[194]A. Rodriguez, J. M. Canosa, and J. Tojo, J. Chem. Thermodyn. **35**, 1321 (2003).
[195]R. E. Rolling and C. J. Vogt, J. Basic Engineering **82**, 635 (1960).
[196]D. I. Sagdeev and G. K. Mukhamedzyanov, Teplo- Massoobmen Khim. Tekhnol. **5**, 21 (1977).
[197]Y. Sato, H. Yoshioka, S. Aikawa, and R. L. Smith, Int. J. Thermophys. **31**, 1896 (2010).
[198]W. G. S. Scaife and C. G. R. Lyons, Proc. R. Soc. London, A **370**, 193 (1980).
[199]A. Schedemann, Master Thesis, Universität Oldenburg, Oldenburg (2009).
[200]W. F. Seyer and A. F. Gallaugher, Trans. Roy. Soc. Can. Sec. 3 **3**, 343 (1926).
[201]H. Shekaari, M. T. Zafarani-Moattar, and M. Niknam, J. Chem. Thermodyn. **97**, 100 (2016).
[202]V. S. Sperkach, P. F. Cholpan, V. N. Sinilo, and A. V. Zolotar, Fiz. Zhidk. Sostoyaniya pp. 110–113 (1979).
[203]T. Takagi and H. Teranishi, Fluid Phase Equilib. **20**, 315 (1985).
[204]Y. Tanaka, H. Hosokawa, H. Kubota, and T. Makita, Int. J. Thermophys. **12**, 245 (1991).
[205]J. Tojo, J. M. Canosa, A. Rodriguez, J. Ortega, and R. Dieppa, J. Chem. Eng. Data **49**, 86 (2004).
[206]J. L. Trenzado, J. S. Matos, L. Segade, and E. Carballo, J. Chem. Eng. Data **46**, 974 (2001).
[207]A. I. Vogel, J. Chem. Soc. **146**, 133 (1946).
[208]A. Watanabe and S. Moroto, Nagoya-Kogyo-Gijutsu-Shikensho-hokoku **27**, 230 (1978).
[209]M. D. Williams-Wynn, P. Naidoo, and D. Ramjugernath, J. Chem. Eng. Data **63**, 4795 (2018).
[210]C. F. Wong and W. Hayduk, J. Chem. Eng. Data **35**, 323 (1990).
[211]J. Wu, Z. Shan, and A. F. A. Asfour, Fluid Phase Equilib. **143**, 263 (1998).
[212]F. Yang, Y. Guo, Y. Xing, D. Li, W. Fang, and R. Lin, J. Chem. Eng. Data **53**, 2237 (2008).
[213]C. Yang, W. Xu, and P. Ma, J. Chem. Eng. Data **49**, 1794 (2004).
[214]C. Yang, W. Yu, and P. Ma, J. Chem. Eng. Data **50**, 1197 (2005).
[215]C. H. Yu and F. N. Tsai, J. Chem. Eng. Data **40**, 601 (1995).
[216]L. Yue, X. Qin, X. Wu, L. Xu, Y. Guo, and W. Fang, J. Chem. Thermodyn. **81**, 26 (2015).
[217]S. S. Bagdasayan, Zh. Fiz. Khim. **38**, 1816 (1964).
[218]T. M. Aminabhavi and K. Banerjee, Indian J. Chem. **40**, 53 (2001).
[219]J. H. Dymond and K. J. Young, Int. J. Thermophys. **1**, 331 (1980).
[220]K. S. Kumar, P. R. Naidu, and W. E. Acree, J. Chem. Eng. Data **39**, 2 (1994).
[221]E. Meeussen, C. Debeuf, and P. Huyskens, Bull. Soc. Chim. Belg. **76**, 145 (1967).
[222]T. D. Terry, R. E. Kepner, and A. D. Webb, J. Chem. Eng. Data **5**, 403 (1960).
[223]K. J. Lee, W. K. Chen, J. W. Ko, L. S. Lee, and C. M. J. Chang, Journal of the Taiwan Institute of Chemical Engineers **40**, 573 (2009).
[224]J. F. Connolly and G. A. Kandalic, Phys. Fluids **3**, 463 (1960).
[225]M. L. McGlashan and D. J. B. Potter, Proc. R. Soc. London, A **267**, 478 (1962).
[226]V. G. Skripka, Zh. Fiz. Khim. **53**, 1407 (1979).
[227]S. D. Zaalishvili, Z. S. Belousova, and V. P. Verkhova, Russ. J. Phys. Chem. **45**, 902 (1971).
[228]P. Navia, J. Troncoso, and L. Romaní, J. Chem. Thermodyn. **40**, 1607 (2008).
[229]A. Griot, R. Philippe, and J. C. Merlin, J. Chim. Phys. Phys.-Chim. Biol. **80**, 507 (1983).
[230]H. Iloukhani, M. Rezaei-Sameti, and J. Basiri-Parsa, J. Chem. Thermodyn. **38**, 975 (2006).
[231]A. Krishnaiah and P. R. Naidu, J. Chem. Eng. Data **25**, 135 (1980).
[232]A. D. Matilla, G. Tardajos, E. Junquera, and E. Aicart, J. Solution Chem. **20**, 805 (1991).
[233]R. A. Orwoll and P. J. Flory, J. Am. Chem. Soc. **89**, 6814 (1967).
[234]K. Shinoda and J. H. Hildebrand, J. Phys. Chem. **65**, 183 (1961).
[235]G. Tardajos, E. Aicart, M. Costas, and D. Patterson, J. Chem. Soc., Faraday Trans. **82**, 2977 (1986).
[236]N. V. Choudary, A. P. Kudchadker, and P. R. Naidu, Phys. Chem. Liq. **16**, 137 (1986).
[237]B. E. de Cominges, T. P. Iglesias, M. M. Piñeiro, J. L. Legido, and M. I. Paz Andrade, Phys. Chem. Liq. **37**, 683 (1999).
[238]E. Junquera, G. Tardajos, and E. Aicart, J. Chem. Thermodyn. **20**, 1461 (1988).
[239]V. N. Kartsev, Zh. Fiz. Khim. **50**, 764 (1976).
[240]J. Jin, F. Shao, H. Dong, and C. Wu, J. Solution Chem. **48**, 82 (2019).
[241]P. Kashyap, M. Rani, and D. P. Tiwari, Asian J. Chem. **32**, 303 (2020).
[242]A. Rodriguez, J. M. Canosa, and J. Tojo, J. Chem. Eng. Data **44**, 666 (1999).
[243]J. W. M. Boelhouwer, Physica **34**, 484 (1967).
[244]M. A. Javed, *Speed of Sound Measurement for Industrially Important Fluids with the Pulse-Echo Technique: Dissertation* (Technische Universität Berlin, 2020).
[245]T. S. Khasanshin, V. S. Samuilov, and A. P. Shchemelev, J. Eng. Phys. Thermophy. **81**, 760 (2008).
[246]A. Badalyan, N. Otpushchennikov, and Y. Shoitov, Izv. Akad. Nauk Arm. SSR Fiz. **5**, 448 (1970).
[247]Y. Zhang, Y. Chen, Y. Zheng, X. He, and M. He, J. Chem. Eng. Data **63**, 102 (2018).
[248]Y. A. Neruchev, Izd. KGPI pp. 67–96 (1969).
[249]Y. A. Neruchev, V. V. Zotov, and N. Otpushchennikov, Russ. J. Phys. Chem. **43**, 1597 (1969).
[250]V. V. Zotov, Y. F. Melikhov, G. A. Mel'nikov, and Y. A. Neruchev, Kurskii gos.pedagog.universitet pp. 1–77 (1995).
[251]A. Blanco, A. Gayol, D. Gómez-Díaz, and J. M. Navaza, Phys. Chem. Liq. **50**, 798 (2012).
[252]P. F. Cholpan, V. S. Sperkach, and L. N. Garkusha, Fiz. Zhidk. Sostoyaniya pp. 79–83 (1981).
[253]Z. S. Ding, J. Alliez, C. Boned, and P. Xan, Meas. Sci. Technol. **8**, 154 (1997).
[254]G. P. Dubey and M. Sharma, J. Mol. Liq. **143**, 109 (2008).
[255]A. Z. Golik and I. I. Ivanova, Russ. J. Phys. Chem. **36**, 951 (1962).

[256]B. González, A. Dominguez, and J. Tojo, J. Chem. Thermodyn. **35**, 939 (2003).
[257]V. H. Hasanov, High Temperature **50**, 44 (2012).
[258]P. Kashyap, M. Rani, S. Gahlyan, D. P. Tiwari, and S. Maken, J. Mol. Liq. **268**, 303 (2018).
[259]T. S. Khasanshin and A. P. Shchemelev, High Temperature **39**, 60 (2001).
[260]S. M. Nayeem, M. Kondaiah, K. Sreekanth, M. Srinivasa Reddy, and D. Krishna Rao, J. Therm. Anal. Calorim. **123**, 2241 (2016).
[261]S. L. Oswal, S. G. Patel, R. L. Gardas, and N. Y. Ghael, Fluid Phase Equilib. **215**, 61 (2004).
[262]M. V. Rathnam, S. Mankumare, and M. S. S. Kumar, J. Chem. Eng. Data **55**, 1354 (2010).
[263]G. A. Ayurov, G. A. Mel'nikov, V. N. Verveiko, and V. M. Tutov, Ul'trazvuk i termodinamiceskie svojstva vescestva pp. 112–125 (1986).
[264]M. A. Kuznetsov, V. E. Kharin, A. A. Gerasimov, and B. A. Grigorev, Izv. Vyssh. Uchebn. Zaved. Neft Gaz **31**, 49 (1988).
[265]I. Czarnota, J. Chem. Thermodyn. **25**, 355 (1993).
[266]I. Czarnota, High Temp. - High Press. **17**, 543 (1985).
[267]K. I. Amirkhanov, B. G. Alibekov, D. I. Vikhrov, and A. M. Kerimov, Teploenergetika **3**, 81 (1964).
[268]K. I. Amirkhanov and V. A. Mirskaya, Viniti, Code 3845-77 p. 1 (1977).
[269]D. Tenji, M. Thol, E. W. Lemmon, and R. Span, Master Thesis, Ruhr-Universität Bochum, Bochum (2018).
[270]K. I. Amirkhanov, G. V. Stepanov, and B. G. Alibekov, *Isochoric Heat Capacity of Water and Steam* (Akad. Nauk SSSR, Dagestanskii Filial, 1969).
[271]A. K. Abas-Zade and A. G. Akhmedov, Dokl. Akad. Nauk SSSR **18**, 15 (1962).
[272]A. G. Akhmedov, Russ. J. Phys. Chem. **44**, 1168 (1970).
[273]L. Andreoli-Ball, D. Patterson, M. Costas, and M. Cáceres-Alonso, J. Chem. Soc., Faraday Trans. **84**, 3991 (1988).
[274]G. C. Benson and P. J. D'Arcy, Can. J. Chem. **64**, 2139 (1986).
[275]C. A. Cerdeiriña, J. A. Miguez, E. Carballo, C. A. Tovar, E. de La Puente, and L. Romaní, Thermochim. Acta **347**, 37 (2000).
[276]T. J. Connolly, B. H. Sage, and W. N. Lacey, Ind. Eng. Chem. **43**, 946 (1951).
[277]M. Costas and D. Patterson, Int. Data Series Sel. Data Mixtures Ser. A **13**, 212 (1985).
[278]Y. Coulier, K. Ballerat-Busserolles, J. Mesones, A. Lowe, and J. Y. Coxam, J. Chem. Eng. Data **60**, 1563 (2015).
[279]L. P. Filippov and L. A. Laushkina, Zh. Fiz. Khim. **58**, 1068 (1984).
[280]B. A. Grigorev, Y. L. Rastorguyev, and G. S. Yanin, Izv. Vyssh. Uchebn. Zaved. Neft Gaz **18**, 63 (1975).
[281]B. A. Grigorev and R. A. Andolenko, Izv. Vyssh. Uchebn. Zaved. Neft Gaz **27**, 60 (1984).
[282]J. P. E. Grolier, A. Inglese, A. H. Roux, and E. Wilhelm, Ber. Bunsen-Ges. Phys. Chem. **85**, 768 (1981).
[283]H. M. Huffman, G. S. Parks, and M. Barmore, J. Am. Chem. Soc. **53**, 3876 (1931).
[284]M. A. Kuznetsov, Russ. J. Phys. Chem. **82**, 145 (2008).
[285]A. Lainez, J. P. E. Grolier, and E. Wilhelm, Thermochim. Acta **91**, 243 (1985).
[286]A. Lainez, M. M. Rodrigo, E. Wilhelm, and J. P. E. Grolier, J. Solution Chem. **21**, 49 (1992).
[287]A. Lainez, M. R. Lopez, M. Cáceres-Alonso, J. Núñez, R. G. Rubio, J. P. E. Grolier, and E. Wilhelm, J. Chem. Soc., Faraday Trans. **91**, 1941 (1995).
[288]A. Lainez, M. Rodrigo, A. H. Roux, J. P. E. Grolier, and E. Wilhelm, Calorim. Anal. Therm. **16**, 153 (1985).
[289]H. Nakai, H. Soejima, K. Tamura, H. Ogawa, S. Murakami, and Y. Toshiyasu, Thermochim. Acta **183**, 15 (1991).
[290]G. S. Parks, H. M. Huffman, and S. B. Thomas, J. Am. Chem. Soc. **52**, 1032 (1930).
[291]S. Perez-Casas, E. Aicart, L. M. Trejo, and M. Costas, Int. Data Series Sel. Data Mixtures Ser. A **2**, 104 (1988).
[292]T. Regueira, F. Varzandeh, E. H. Stenby, and W. Yan, J. Chem. Thermodyn. **111**, 250 (2017).
[293]A. H. Roux, J. P. E. Grolier, A. Inglese, and E. Wilhelm, Ber. Bunsen-Ges. Phys. Chem. **88**, 986 (1984).
[294]H. Soejima, H. Nakai, K. Tamura, H. Ogawa, S. Murakami, and Y. Toshiyasu, Thermochim. Acta **177**, 305 (1991).
[295]L. M. Trejo, M. Costas, and D. Patterson, Int. Data Series Sel. Data Mixtures Ser. A **19**, 9 (1991).
[296]J. S. Emampour, A. Morsalo, S. A. Beyramabadi, M. R. Bozorgmehr, and K. Khakzadan, Int. J. Phy. Sci. **6**, 5731 (2011).
[297]V. Arp, J. M. Persichetti, and G. B. Chen, J. Fluids Eng. **106**, 193 (1984).
[298]G. Venkatarathnama and L. R. Oellrich, Fluid Phase Equilib. **301**, 225 (2011).
[299]E. Grüneisen, Ann. Phys. **344**, 257 (1912).
[300]E. W. Lemmon, I. H. Bell, M. L. Huber, and M. O. McLinden, *NIST Standard Reference Database 23: Reference Fluid Thermodynamic and Transport Properties-REFPROP* (2018).
[301]R. Span, R. Beckmüller, S. Hielscher, A. Jäger, E. Mickoleit, T. Neumann, S. M. Pohl, B. Semrau, and M. Thol, *TREND. Thermodynamic Reference and Engineering Data 5.0* (2020).
[302]I. H. Bell, J. Wronski, S. Quoilin, and V. Lemort, Ind. Eng. Chem. Res. **53**, 2498 (2014).